energies

MDPI

Review

All-Perovskite Tandem Solar Cells: From Certified 25% and Beyond

Nour El Islam Boukortt [1], Claudia Triolo [2,3], Saveria Santangelo [2,3] and Salvatore Patanè [3,4,*]

[1] Electronics and Communication Engineering Department, Kuwait College of Science and Technology, Road N. 7, Doha 13113, Kuwait
[2] Dipartimento di Ingegneria Civile, dell'Energia, dell'Ambiente e dei Materiali (DICEAM), Università "Mediterranea", Via Zehender, Loc. Feo di Vito, 89122 Reggio Calabria, Italy
[3] National Reference Center for Electrochemical Energy Storage (GISEL), Consorzio Interuniversitario Nazionale per la Scienza e Tecnologia dei Materiali (INSTM), Via Giusti 9, 50121 Firenze, Italy
[4] Dipartimento di Scienze Matematiche e Informatiche, Scienze Fisiche e Scienze della Terra (MIFT), Università di Messina, Viale Stagno d'Alcontres 31, 98166 Messina, Italy
* Correspondence: patanes@unime.it

Abstract: Perovskite-based solar cells are a promising photovoltaic technology capable of offering higher conversion efficiency at low costs compared with the standard of the market. They can be produced via a thin film technology that allows for considerable environmental sustainability, thus representing an efficient, sustainable, flexible, and light solution. Tandem solar cells represent the next step in the evolution of photovoltaics (PV). They promise higher power conversion efficiency (PCE) than those currently dominating the market. The tandem solar cell design overcomes the limitations of single junction solar cells by reducing the thermal losses as well as the manufacturing costs. Perovskite has been employed as a partner in different kinds of tandem solar cells, such as the Si and CIGS (copper indium gallium selenide) based cells that, in their tandem configuration with perovskite, can convert light more efficiently than standalone sub-cells. This brief review presents the main engineering and scientific challenges in the field. The state-of-the-art three main perovskite tandem technologies, namely perovskite/silicon, perovskite/CIGS, and perovskite/perovskite tandem solar cells, will be discussed, providing a side-by-side comparison of theoretical and experimental efficiencies of multijunction solar cells.

Keywords: tandem solar cell; perovskite; organic solar cells; power conversion efficiency (PCE)

Citation: Boukortt, N.E.I.; Triolo, C.; Santangelo, S.; Patanè, S. All-Perovskite Tandem Solar Cells: From Certified 25% and Beyond. *Energies* **2023**, *16*, 3519. https://doi.org/10.3390/en16083519

Academic Editor: Adalgisa Sinicropi

Received: 11 March 2023
Revised: 5 April 2023
Accepted: 12 April 2023
Published: 18 April 2023

1. Introduction

In the last few years, the growing interest in substituting fossil-based fuel with renewable energies has pushed up PV technologies towards new materials and designs to improve efficiency and limit costs [1,2]. During 2021, all the world's regions increased solar photovoltaics, despite the tough post-COVID economic context of disrupted supply chains and more expensive solar system components. Data from the International Renewable Energy Agency (IRENA) released on 11 April 2022 show that, at the end of 2021, the installed solar capacity worldwide reached 843.1 GW, with an increase of 133.6 GW, surpassing that of wind, which was 824.9 GW for the same period. Energy prices, already high in the electricity market in 2021, rose even more due to the Russian invasion of Ukraine on 24 February 2022, generating an epochal change in governments' approach to the energy issue and spurring even more the so-called ecological transition, in which photovoltaics are one of the main protagonists.

Among the many technologies for photovoltaics, crystalline silicon is undoubtedly the most mature and the most commercially suitable for the modern market. For the past several decades, silicon solar cells have been the main driving force in PV technology due to the abundance and environmentally friendly nature of silicon, as well as its high

stability and low cost. Nevertheless, this semiconductor suffers from several drawbacks that intrinsically limit cell efficiency. For example, the silicon spectral quantum efficiency and the air mass (AM) solar spectrum do not match; consequently, only a little amount of long wavelength sunlight is absorbed. Typically, the above problem is solved by designing a relatively thick silicon structure that allows for greater photon absorption. However, at the same time, this introduces inevitable conversion efficiency losses due to the non-radiative recombination process of the photo-generated charge carriers that must travel from the depletion region to the electrical contacts. All these constraints, also taking into account the Auger effect, make the maximum practical achievable efficiency about 30% [3–6]. One of the potential technologies for next-generation silicon solar cells is the silicon heterojunction (SHJ). When compared with industrial homojunction silicon solar cells, SHJ solar cells exhibit a better power transfer efficiency, lower manufacturing temperatures, and a lower temperature coefficient. The term heterojunction refers to the fact that the P–N junction consists of silicon layers with two different morphologies: a p-type amorphous silicon region and the n-doped crystalline silicon absorber. The first silicon-based heterojunction device was made in 1983 and had an efficiency greater than 12% [7]. In the early 1990s, Sanyo developed the HIT (heterojunction with intrinsic thin layer) solar cell. Its design dramatically reduces the surface recombination thanks to an amorphous Si buffer layer inserted between the doped emitter and the substrate [8]. The most recent world record for a silicon solar cell was recently set by the Kaneka Corporation, which obtained an efficiency of up to 26.7% for a 79 cm^2 solar cell [9]. This finding is approaching the theoretical top limit of 29% for single junction silicon solar cells [10] and pushes up the research toward novel configurations employing different materials to approach a higher efficiency at lower or at least reasonable costs. A well-known strategy for improving efficiency is the multijunction design that uses multiple junctions, made with different semiconductors each tuned to absorb a different region of the solar spectrum.

Multijunction devices' topology includes an upper cell made of wider bandgap semiconductors able to catch the high-energy photons, allowing the lower-energy photons to pass through. Then, to capture photons at longer wavelengths, one or more junctions with smaller bandgap semiconductors are placed beneath the top junction. The ultimate theoretical efficiency increases with the number of junctions stacked on top of each other.

Early research into multijunction devices exploited semiconductors such as gallium indium phosphate (GaInP), gallium indium arsenide (GaInAs), and gallium arsenide (GaAs). At present, a 47.1% solar conversion efficiency has been demonstrated using a monolithic, series-connected, six-junction inverted metamorphic structure with alloys of III–V semiconductors and operating under the direct spectrum at 143 suns concentration.

Building these junctions requires the reduction of the threading dislocations in lattice-mismatched III–V alloys, avoiding the phase segregation in metastable quaternary III–V alloys, and controlling the dopant diffusion in complex structures [11], resulting in a more expensive technology compared with the standard silicon-based one.

Indeed, multijunction devices have mostly been employed in space, where the use of this somewhat expensive solar technology is allowable to reduce weight and dimensions. For terrestrial applications, concentrating optics based on Fresnel lenses may be used to increase power output, lowering the costs. Dual-axis sun tracking is needed when using concentrating optics, which adds to the system's cost. The literature is teeming with articles describing solar cells with different trick topologies that improve overall efficiency.

Recently, efficiencies of 39.5% have been achieved integrating a thick GaInAs/GaAsP strain-balanced quantum well (QW) into a triple-junction inverted metamorphic multijunction device, consisting of a GaInP upper cell, a GaInAs/GaAsP QW middle cell, and a mismatched lattice GaInAs lower cell [12].

This work briefly reviews the main engineering and scientific challenges in tandem technology, which, at present, is the most promising PV cell architecture for improving the photon absorption and the PCE. Keeping the perovskite materials as the active layer, perovskite/silicon, perovskite/CIGS, and perovskite/perovskite tandem solar cells will be

discussed, providing a side-by-side comparison of theoretical and experimental efficiencies of multijunction solar cells. The aim is to provide a critical analysis of state-of-the-art devices, which are largely dominated by perovskite/silicon tandem solar cells that historically were the first cells produced and studied. The drawbacks of these cells have been the starting point for the development of a new generation of heterojunction solar cells. Among them, perovskite/CIGS and perovskite/perovskite tandem solar cells will be discussed, and their limitations and the challenges for their future development considered.

2. Tandem Architecture

The tandem structure consists of two solar cells mechanically coupled one over the other in order to maximize the photon abortion. In addition, the combination of the two materials maximizes production of a high photo-voltage, equal to the sum of the voltages generated by the two individual cells, thus producing greater efficiency than a single solar cell.

As shown in Figure 1, the device architecture cell can be a monolithic device (2T tandem cell), where the upper wide bandgap cell is fabricated above the lower narrow bandgap cell; in the second configuration (4T tandem cell), a mechanical stacking optically couples the two sub-cells that are electrically isolated.

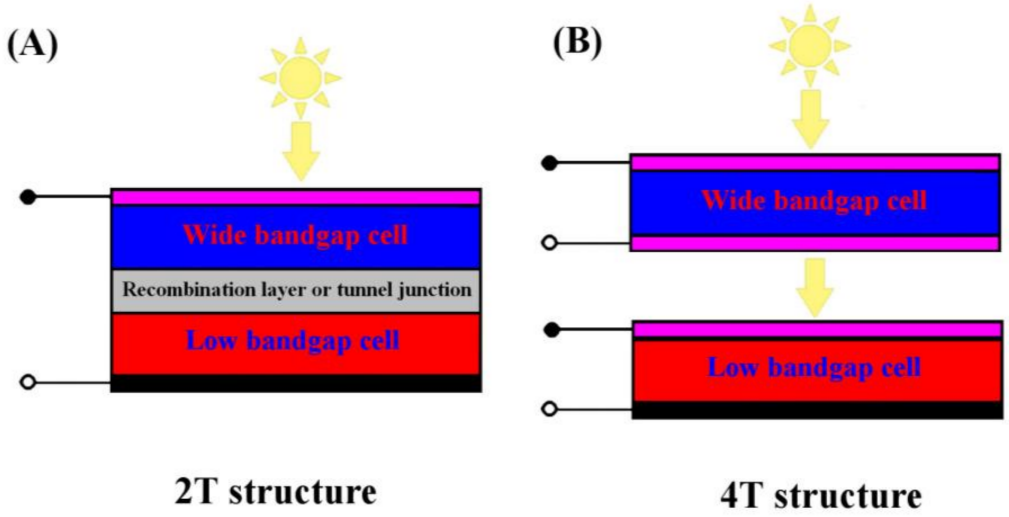

Figure 1. (**A**) 2T and (**B**) 4T topologies. The first typically consists of a monolithic structure, where the layer connecting the two cells plays the role of a recombination layer or works as a tunnel junction. The 2T structure is a mechanical stacking of two separate cells with different bandgap active layers.

These two architectures are not equivalent both from an electrical and a constructive point of view (Figure 2). A 2T device needs the current matching of the top and bottom cells as the two sub-cells are connected in series and the lower current sub-cell will limit the overall short-circuit device current. Conversely, the 4T tandem solar cells do not require current matching because the two cells are not electrically connected. Therefore, maximizing the efficiency of both top and bottom cell can boost the overall device performance of a 4T tandem device. The 2T architecture requires a precise design strategy to collect the charges that must pass through the entire device to reach the electrodes; for example, the upper and lower cells can be interconnected by thin tunnel junction [13]. On the other hand, the 4T structure requires integrating at least one electrode between the two cells, and this electrode must let the infrared photons pass through so that they can reach the lower cell. Thin Ag films or nanowires have been used for this purpose, but more complex (such as multilayer metallic/dielectric) structures may improve the performance [14,15]. A simpler approach consists of using a photon down conversion mechanism, where a standard silicon-based solar cell is covered by a thin film that can absorb blue light and re-emit photons at a longer

wavelength, allowing red and infrared solar light to pass towards the rear cell, effectively increasing the energy produced [16].

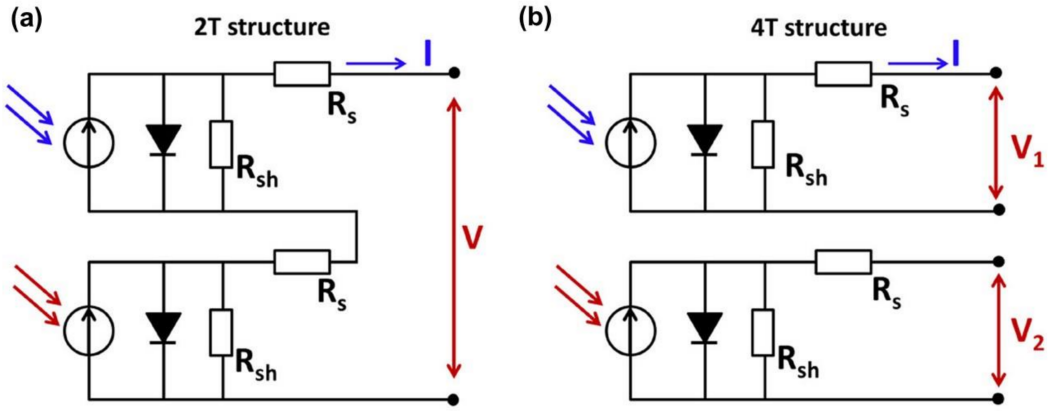

Figure 2. Equivalent circuit models of 2T (**a**) and 4T (**b**) tandem cells. In these schemes, I, R_{sh}, and R_s indicate the generated photocurrent, the shunt, and the series resistances, respectively. Finally, V is the output voltage. Blu and red arrows indicate the spectral response of the top and bottom cells, that work in the visible (400–800 nm) and IR (800–1100 nm) ranges, respectively. (Figure reprinted from Cheng et al. [17], Copyright (2023) with permission of SusMat).

3. Perovskite Group Materials

The term "perovskite" describes a group of materials with cubic and rhomboidal shapes, and a crystal structure, and it was named in honor of the 19th century Russian mineralogist Lev Perovski. The 'true perovskite' mineral is composed of calcium, titanium, and oxygen in the form of $CaTiO_3$. However, "perovskite" usually refers to a structure with the generic form ABX_3, with variable composition and the same crystalline structure. A and B can be a combination of different organic and inorganic cations, and X is a smaller halogen anion (usually oxide) that binds to both cations (Figure 3).

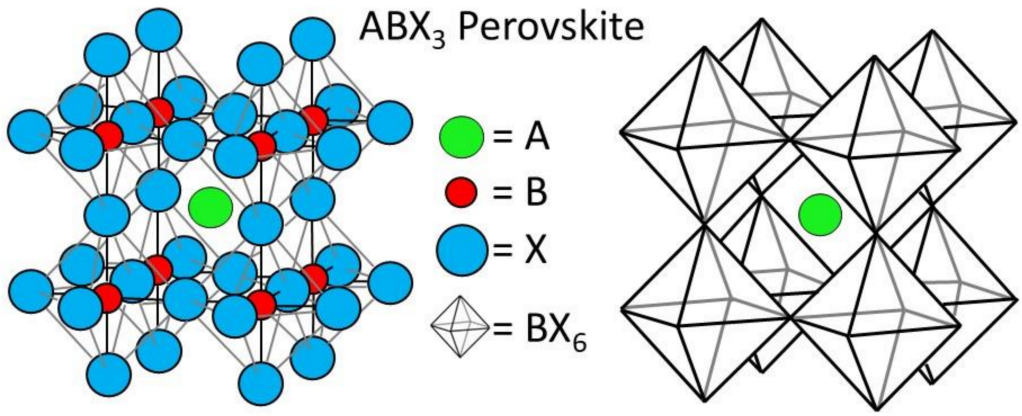

Figure 3. Crystal lattice of the ABX_3 perovskite structure.

Hence, this class of material exhibits a large variety of possible structural modifications and variants [18]. A limited number of perovskites may be found in nature, mainly as oxides with the majority being silicates, but they can also exist as fluorides, arsenides, hydroxides, chlorides, and intermetallic compounds. While there are only a few naturally occurring perovskite minerals, synthetic perovskites can span across the entire periodic table and can have a wide variety of complex formulas, including hybrid organic–inorganic perovskites, metallic perovskites, metal-free perovskites, and even noble gas-based perovskites. Perovskites can exhibit a wide range of intriguing features, including superconductivity, giant magnetoresistance, spin-dependent transport (spintronics), and catalytic capabilities,

depending on which atoms or molecules are employed in the structure [18–20]. As a result, perovskites offer an intriguing research environment for physicists, chemists, and material scientists. Since the most efficient perovskites are semiconducting lead metal halides with a tunable bandgap, this family of crystals holds great promise for use in many nanotechnology applications, such as nanostructured solar cells.

Indeed, due to their extraordinary efficiency at absorbing photons, interest in perovskite-based solar cells has skyrocketed in recent years. It was immediately clear that perovskites are very flexible materials with which it is possible to obtain high conversion efficiencies at low costs as they can be produced with relatively simple manufacturing by cheap processes.

Moreover, long carrier separation lifetime, fast charge separation, a broad absorption spectrum, a larger mean free path of electrons and holes, and more, make perovskites very suitable for building solid-state solar cells.

In 2009, the literature reported the first example of a photovoltaic cell based on the organic–inorganic lead halide perovskite compounds $CH_3NH_3PbBr_3$ and $CH_3NH_3PbI_3$, with an efficiency of 3.8% and a photovoltage of 0.96 V, respectively [21].

The basic structure of a perovskite solar cell consists of a hole transporting layer (HTL), an electron transporting layer (ETL), a transparent electrode working as an anode (fluorine-doped tin oxide, FTO, or indium tin oxide, ITO), and a metal (Figure 4). In the resulting sandwich structure, the photogenerated electrons and holes coexist in $CH_3NH_3PbX_3$ absorber material and travel to the selective contacts, where they are collected separately. By altering the material composition, perovskites can be tuned to respond to various solar spectrum colors, and a number of formulations have proven to be highly effective. The efficiency of perovskite solar cells has increased dramatically in recent years, from about 3% in 2009 to over 25% in 2021 [22,23]. In 2012, Professor Henry Snaith at the University of Oxford demonstrated 10% power conversion efficiencies by hybrid solar cells based on meso-super structured organometal halide perovskites [24]. Only two years later, Snaith obtained a conversion efficiency of up to 17%. For silicon-based solar cells, it took 20 years of research to reach these values. Although perovskite solar cells have achieved high efficiency very quickly, some issues still need to be overcome before they can become commercially competitive. At the same time, however, these materials show rather short lifetimes, which is not very compatible with solar cell technologies, as they tend to break down under direct sunlight, reducing the cells' efficiency over time. This point has been intensively studied with different techniques over the last few years. A well-known mechanism responsible for perovskite degradation involves humidity and methylammonium (MA) groups, since water can hydrogen bond with the amine moiety. The Raman activity of MA is very sensitive to structural distortions of the inorganic structure and can be used to control the quality of the material. [25]. People have tried to fix this durability issue by adding bulky molecules [26], old pigments [27], carbon nanodots [28], 2D additives [29], chili compounds [30], or quantum dots [31]. UCLA researchers identified a mechanism for how this deterioration takes place. Ironically, it results from a surface treatment intended to remove flaws and boost performance. The scientists discovered that coating the surface with an organic ion layer can lead to the formation of traps, causing energy-bearing electrons to gather on the surface. As a result, the arrangement of the perovskite atoms becomes unstable, eventually leading to their rupture. The team suggested solving the issue by mixing positive and negative ions in the surface treatment. Solar cell prototypes treated with the above approach maintained 87% of their efficiency after more than 2000 h, outperforming untreated cells, which fell to 65% efficiency in the same conditions [32].

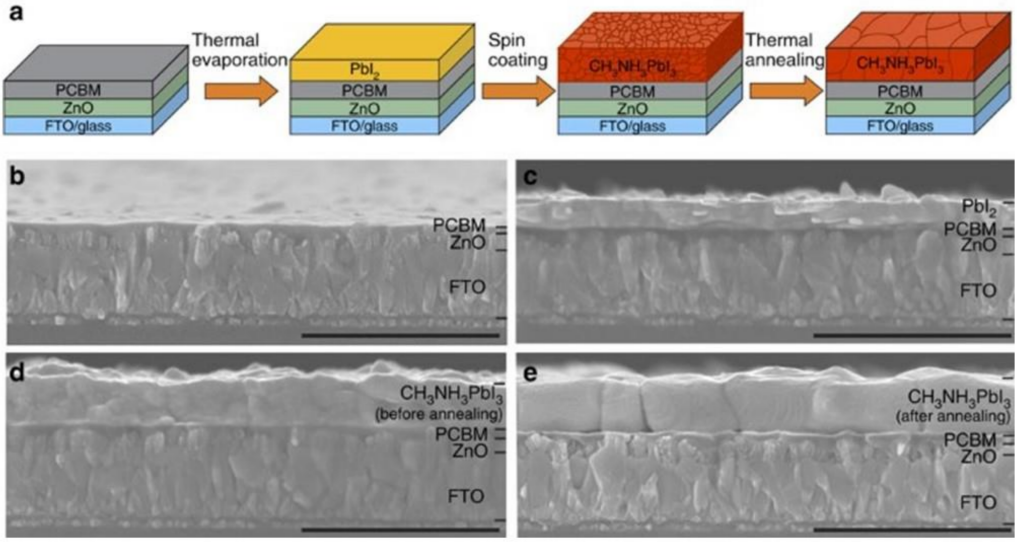

Figure 4. (**a**) Preparation steps of perovskite-based device; (**b**–**e**) the cross-sectional SEM images of the sample for each preparation step. (Figure reprinted from Fu et al. [33], copyright (2023) with permission of Nature Communications).

4. Perovskite/Silicon Solar Cells

Tandem cells can overcome the thermodynamic efficiency barrier that limits the well-stated silicon and cadmium-telluride (CdTe) solar technologies. However, tandem cells are costly, and are therefore currently exclusively employed for power generation in space or for very special applications. To make mass use possible, novel generation of affordable tandem cells is required. The most popular low-cost tandem option now being developed combines a silicon bottom cell with a hybrid perovskite top cell.

The use of perovskite as a tandem top cell has several advantageous features. For one, perovskites have adjustable semiconductor bandgap energies, which is a crucial factor in determining the optical absorption range of a semiconductor that adds flexibility in a device design. Perovskites' absorption is quite low in the infrared region of the solar spectrum, which helps the invisible photons to reach the bottom silicon cell, boosting efficiency. Furthermore, perovskites work at very high voltages. This is important because the high transparency of the cell to infrared light also reduces its electric current. However, this limitation is compensated by a high working voltage, ensuring high power and efficiency. Moreover, the silicon cell absorbs infrared very well, and its technology is well known and guarantees long life and stability. Research on perovskite–silicon solar cells has achieved many world records, the latest being by Oxford PV, a startup which reached 29.5% [34,35]. The same company has prototyped full-sized modules, and promising field outcomes have been recorded [36]. The first perovskite-on-silicon 4T solar cell with a PCE of 17.9% was demonstrated by Bailie and coworkers in 2014 [37]. To avoid harming the underlying layer, they used a solventless strategy to transfer the transparent Ag nanowires (NWs) contact mechanically from flexible polyethylene terephthalate (PET) onto the top of 2,2′,7,7′ Tetrakis (N,N-di-4-methoxyphenylamino)-9,9′-spirobifluorene (spiro-OMeTAD). The resulting electrode had an overall transmittance of 87–90% and the upper semitransparent half-cell demonstrated an efficiency of approximately 13%, with a transmittance of 55–77% between 800 and 1200 nm. However, the use of silver is not recommended because it can give rise to the formation of silver iodides, degrading the structure of the perovskite and the cell performance [38]. The above clearly states that, as a general rule, the right choice of electrodes plays an important role in designing the cell structure.

A further challenge consists of the fact that, by reaching high temperatures during electrode deposition, the perovskite active layer is damaged, therefore a low-temperature process has been proposed to build semitransparent planar perovskite solar cells. It consists of sputtering hydrogenated indium oxide (In_2O_3:H) to make the transparent rear

electrode. The perovskite is prepared by thermal evaporation of PbI_2 [39] and spin coating of CH_3NH_3I. Finally, the structure undergoes a 2 h thermal treatment at 50 °C; therefore, the highest temperature reached during the process is as low as 50 °C. The cell is finished with a spin coated ∼200 nm Spiro-OMeTAD thin film and a back contact by thermally evaporated MoO_3, and room-temperature-sputtered In_2O_3:H. The proposed hybrid construction method produces higher quality perovskite thin films and allows for improved electron collection [33]. A general issue in developing perovskite solar cells is the top and the bottom (in 4T configuration) transparent electrodes. Transparent conductive oxides (TCO) deposited by sputtering have been largely used for this purpose. The sputtering may damage the perovskite layer, hence MoO_x and WO_x are used as buffer layers to protect the underlying structures from TCO deposition [17]. ITO was used by Löper and coworkers to protect the underlying layers from sputtering damage with a MoO_3 buffer [40]. The total efficiency of the 4T multijunction solar cell was 13.4%. Compared with an opaque single junction cell with a MoO_x/Ag electrode, which had an efficiency of 11.6%, the semitransparent perovskite top cell showed a performance of 6.2%. The improved sheet resistance and decreased reflectance of the ITO transparent electrode were the key contributors to the difference. Given that, in a multijunction device, the absorption of the transparent contacts accounts for most of the optical losses, the layer's thickness ought to be decreased. However, as the thinner device results in reduced conductivity, which lowers voltage and FF loss, a careful balance between electrical and optical losses is required.

Duong et al. [41] improved sputtered ITO thin film to be used for both back and front contacts. They built a device using methylammonium perovskite ($MAPbI_3$) and obtained an efficiency that exceeded 12% and a transmittance above 80% in the range of 800–1000 nm. One of the most popular ETLs is titanium oxide (TiO_2), which has been extensively employed in perovskite solar cells due to its good electronic and optical characteristics, and chemical resistance, as well as its compatibility with a wide range of deposition techniques [24,42,43]. Peng at al. [44] showed that doping with indium improves both the band alignment at the electron transport perovskite layer interface and the conductivity of the transport layer compared with pure TiO_2. They obtained a semitransparent perovskite cell with 16.6% efficiency, made using a mixed perovskite based on MA and formamidinium (FA). The tandem with an interdigitated back contact (IBC) silicon cell had an efficiency of 24.5%. The best efficiency in photon capturing is achieved by matching the optical bandgap of the two sub-cells. According to suitable optical simulations, the ideal top cell should have a bandgap of 1.7 eV while the bottom cell has a fixed bandgap of 1.1 eV (silicon) [45–47]. Unfortunately, $MAPbI_3$, a widely used perovskite, has a bandgap of 1.55 eV, which does not match well for perovskite–Si multijunction solar cells [24,48,49]. A higher bandgap perovskite could be produced by partially substituting bromide for iodide in the $MAPbI_3$ perovskite. However, these mixed halide MA-based perovskites when illuminated undergo phase segregation, and the cell efficiency is reduced [50–54]. Duong et al. [55] produced a perovskite cell with improved light stability and a bandgap of 1.73 eV by adding Rb cations to a multication perovskite. The cell structure consisted of a MoO_x(10 nm)/ITO (40 nm) transparent electrode. The sheet resistance of the rear ITO contact was as high as 160 $\Omega \cdot cm^{-1}$ and was improved by depositing some Au fingers with shading of 3%, as ITO annealing is not compatible with perovskite quality. Moreover, an anti-reflection coating consisting of 150 nm thick MgF_2 was deposited on the ITO back side and reduced the sample reflectance to less than 5% across nearly the entire spectrum. The best semitransparent cell exhibited an efficiency of 16% and a noticeable transparency of about 84% in the wavelength range between 720 and 1100 nm. As a result, the mechanically stacked multijunction had a total efficiency of 26.4% [54]. Another method to build the transparent contact consists of the thermal vacuum deposition that allows production of ultrathin metal films with low sheet resistance and does not require a buffer layer before deposition. However, the quality of the obtained film greatly depends on the roughness of the substrate on which the film is deposited, and hence it needs to be controlled. Chen et al. [56] studied the efficiency, in term of

conductivity and transparency, of an Au, Cu, and Au/Cu bilayer with different thicknesses, and fabricated semitransparent perovskite solar cells using 500 nm thick smooth $MAPbI_3$ films. They found that the best efficiency was obtained employing the Au/Cu (7 nm/1 nm) bilayer, and the cell performed an open-circuit voltage (V_{OC}) of 1.08 V, a short-circuit current density (J_{SC}) of 20.6 mA cm^{-2}, a fill factor (FF) of 74.1%, and a PCE of 16.5%. Moreover, they built the tandem configuration in the four-terminal configuration with infrared-enhanced silicon heterojunction cells and obtained a total efficiency of 23% [56]. Most of the literature proposes small-area examples to demonstrate efficiency records. Indeed, scaling up maintaining efficiency is another problem, as large-area devices undergo increasing sheet resistance of electrodes and short circuits through the perovskite film. Jaysankar et al. [57] built a four-terminal semitransparent perovskite module with an IBC silicon device of the same size. The aperture area PCE of the 4T perovskite-c-Si module was 20.2%. This study offers a practical method for producing perovskite-c-Si multijunction solar cells in large areas for commercial use [57].

The 2T configuration consists of a monolithic device, where the top sub-cell is directly deposited onto the bottom one.

The above design requires only one transparent electrode; hence, this aspect is much simpler compared with the 4T multijunction device, as the number of fabrication steps, as well as the manufacturing cost and the parasitic absorption loss in the transparent electrodes, are reduced. However, the monolithic tandem requires a process compatibility between the upper and lower cells and, furthermore, both sub-cells, connected in series, should be designed to give the same current at the maximum power point. Usually, the 2T design includes an HIT or passivating tunnel oxide (polySi/SiO_x) integrated in perovskite/c-Si. The tandem structure is possible in two different configurations: the p–i–n perovskite/c-Si and the n–i–p perovskite/c-Si. Figure 5 displays the schemes of perovskite solar cells in planar regular (n–i–p), and planar inverted (p–i–n) architectures. The HTL, such as Spiro-OMeTAD in the n–i–p perovskite/c-Si structures, is responsible for huge absorption of light, limiting the overall performance [13,55,58]; therefore, the research has focused on p–i–n perovskite/c-Si tandems, and this strategy has allowed the realization of monolithic p–i–n perovskite/c-Si tandem solar cells with an efficiency of 23.6% [59]. Mailoa et al. [60] in 2015 built a monolithic multijunction solar cell with an efficiency of up to 13.7% by growing a mesoporous $MAPbI_3$ perovskite cell on a n-type silicon cell and employing an Ag NWs thin film as a transparent electrode. The carrier recombination between the two sub-cells was aided by a tunnel junction deposited by plasma-enhanced chemical vapor deposition (PECVD) of heavily doped n++ hydrogenated amorphous silicon (a-Si:H) [13]. Due to their high efficiency, straightforward manufacturing process, a high V_{OC}, and high energy density, SHJ solar cells have attracted widespread attention [60–66]. In terms of PCE, monolithic two-terminal perovskite–silicon tandem solar cells (PSTSCs) have reached 31%, outperforming traditional crystalline–silicon single-junction solar cells [67]. A fine-tuning of the layers is needed to achieve a better optical performance [66,68,69], and, to achieve the best overall efficiency, optimization of the contact layers [70], use of additives [28,29], and adjustment of the perovskite composition [71] or deposition [72] is required. Another key point, supported by extensive numerical studies, concerns the optical efficiency of the device, which can be improved using textured interfaces that capture photons, allowing high PCEs [73]. The simulations indicate that, compared with planar solar cells, the PCE can be substantially improved [74], as oblique and scattered photons are easily absorbed by the textured surface, strongly affecting the energy yield calculations. Random pyramidal textures, obtained by potassium–hydroxide etching, with a size of some micrometers, are frequently used for light harvesting in silicon solar cells. However, the performance of PV devices strongly depends on the recombination of the charge carriers, and further improving of perovskite absorbers is needed [22]. Recently, different methods for implementing light harvesting PSTSC have been proposed, by modifying the perovskite deposition method while maintaining the pyramidal texture [65,75–77], by modifying it so that perovskite solution processing is possible [66,78–82], or by replicating a pyramidally

textured surface on a polydimethylsiloxane (PDMS) layer instead of using the textured silicon bottom cell [83]. Tockhorn et al. [84] modified the texturing of the front surface of the silicon sub-cell, building a sinusoidal nanostructure by a more complex procedure consisting of ultraviolet nanoimprint lithography, reactive ion etching, and wet chemical etching. The resulting nanotexture had a 300 nm peak-to-valley height, a 750 nm period, and a hexagonal lattice, and was completely covered by a 500–600 nm thick perovskite thin film deposited by spin coating. On the rear side of the structure, a silver back reflector was integrated that reduced the parasitic absorption losses, achieving a certified PCE of 29.80% [84]. It is easy to understand that, when constructing a tandem structure, the processes that involve the realization of the thin layers must be compatible with each other. Furthermore, as in the 2T configuration where the current is limited by the bottom cell, its efficiency is very important, and improving its infrared response could further push up the overall performance of the cell. In this frame, so-called SHJ solar cells have drawn a lot of interest thanks to their high efficiency, approaching 26%, a high V_{OC}, and straightforward low temperature manufacturing process [60,61,85]. SHJs use c-Si wafers as optical absorbers and employ bilayers of doped/intrinsic a-Si:H to create passivating contacts. However, the passivation quality of the a-Si:H/c-Si interface decreases at high temperatures, which makes SHJ cells unstable beyond 200 °C. In contrast, the highest efficiency mesoporous perovskite employs TiO_2 sintered over 450 °C, making the process inappropriate for building a SHJ cell. An example of a device including a mesoporous TiO_2 film is shown in Figure 6. Different deposition methods, such as spin coating [86], spray pyrolysis [87–89], oblique electrostatic inkjet [90], electrodeposition [91], inkjet printing [92], atomic layer deposition (ALD) [93], and chemical bath deposition [94], have been used by several groups to develop ETLs based on a TiO_2 compact layer. ETLs also can be made using spray pyrolysis or spin coating top-down methods, though the PCE of such manufactured devices can differ greatly because these techniques are quite sensitive to the control parameters. Reactive sputtering was used by Alberti et al. [95] to create a low-temperature nanostructured TiO_2 layer; the method allowed a maximal PCE of 15% to be achieved without the use of surface treatments or additional layers. In 2020, a low-temperature (TiO_x) film was obtained via a low-temperature (80 °C) chemical bath deposition procedure. The film, when used as a high-quality ETL for planar PSCs, demonstrated an efficiency as high as 14.5% compared with standard TiO_2 compact ETL that performed at 15.5% [96]. Using a planar perovskite sub-cell with a compact ETL synthesized under benign circumstances is another potential remedy for this problem. Another possible solution to this issue consists of building a planar perovskite sub-cell with a compact ETL, as proposed by Albrecht et al. [97]. In 2016, they fabricated a monolithic tandem cell with 18% efficiency consisting of a perovskite top cell grown on a silicon heterojunction bottom cell. They fabricated the perovskite semitransparent sub-cell at a temperature below 100 °C, replacing the high-temperature mesoporous TiO_2 with a SnO_2 thin film deposited by ALD. The transparent top contact was a multilayer consisting of spiro-OMeTAD, MoO_3 and sputtered ITO. The SnO_2 and the underlying ITO worked as a recombination layer between the two sub-cells. A LiF thin film deposited on the top contact served as an antireflective coating [97]. The requirement to hold the temperature as low as possible can also be satisfied by synthesizing organic polymeric thin film as ETL.

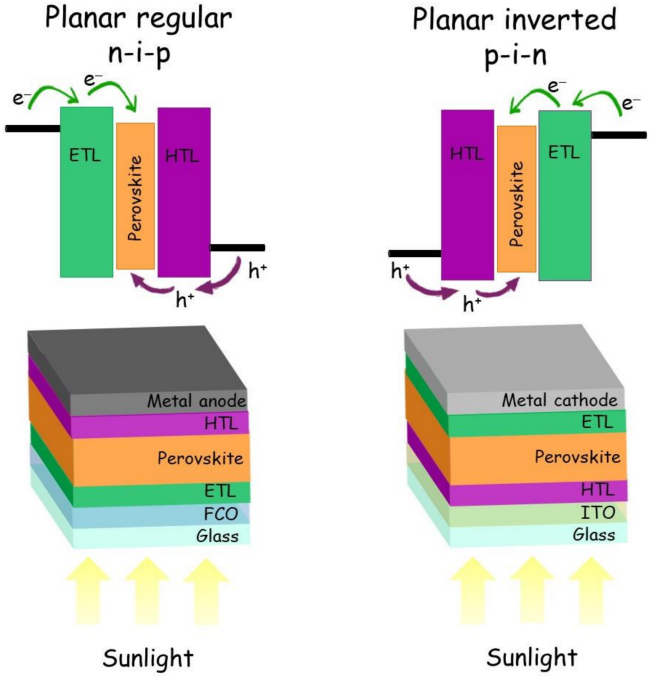

Figure 5. Schematic of perovskite solar cells in planar regular (n-i-p), and planar inverted (p-i-n) architectures.

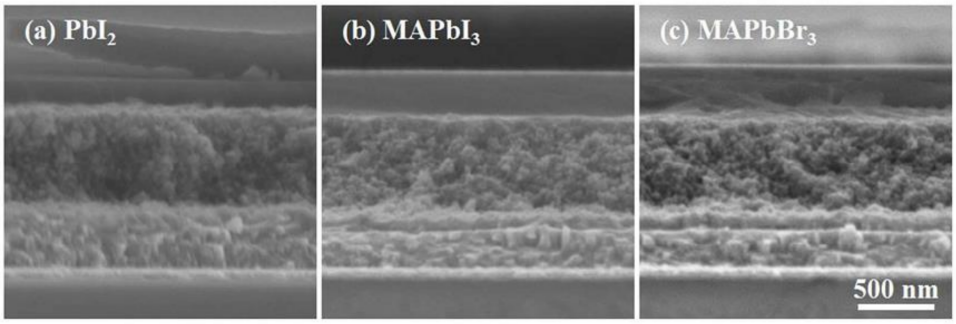

Figure 6. Cross-section SEM images of (**a**) PbI_2, (**b**) $MAPbI_3$, and (**c**) $MAPbBr_3$ deposited on a mesoporous TiO_2 film. (Figure reprinted from Zhao et al. [89], copyright (2023) with permission of Faraday Discussions, RSC).

Reduced graphene oxide (rGO) has been added to [6,6]-Phenyl-C61-butyric acid methyl ester (PCBM), using both the $CH_3NH_3PbI_3-xClx$ perovskite deposited through the one-step method, and the $CH_3NH_3PbI_3$ deposited by a two-step spin coating process. The use of rGO as an additive increases the PCBM conductivity, improving the J_{SC} and FF, while the surface traps are reduced, resulting in a higher V_{OC}. Furthermore, the rGO helps to stabilize the PCBM/perovskite interface, suppressing the degradation rate under continuous solar [98]. Werner et al. used a polyethylenimine (PEIE)/phenyl-C61-butyric-acid-methyl-ester (PCBM) bilayer as the ETL to create a low-temperature processed planar perovskite cell [99]. An $MAPbI_3$ perovskite layer was built by a two-step deposition consisting first of a thermal deposition of PbI_2 on a PCBM, and then a solution of MAI dissolved in isopropanol was spin coated onto the PbI_2 layer and annealed at 100 °C for 30 min. To obtain a uniform, hole-free, flat perovskite layer, a tiny amount of 2-methoxyethanol was added to the MAI precursor. The recombination layer consisted of a sputtered IZO (indium zinc oxide) film, and spiro-OMeTAD worked as the hole transport material. The transparent top electrode was obtained by depositing hydrogenated indium oxide/indium tin oxide (IO:H/ITO) on the spiro-OMeTAD and covering it with a MoO_x buffer layer. The resulting monolithic integrated 2T solar cell exhibited a steady-state

efficiency of 21.2% and an aperture area of 1.22 cm^2. By integrating a SHJ cell optimized to work in the infrared region of the spectrum with a cesium-doped $FAPbI_3$ perovskite cell in a 2T structure, Bush et al. [59] obtained an efficiency of 23.6%, with an active area of 1 cm^2.

The structure should have been closed by an ITO top electrode; however, when ITO is being sputter deposited, the organic and perovskite layers can be damaged. To avoid this occurrence, they inserted a bilayer of SnO_2/ZTO as the ETL. This buffer was enough to avoid damage. The increased thermal stability and resistance to humidity allowed the deposition of SnO_2 with ALD techniques. The ITO top electrode was directly sputtered onto the SnO_2/ZTO, avoiding the use of a MoO_x buffer layer as it reacts with the iodine at the interface with the perovskite, decreasing the lifetime [100]. The infrared absorption was enhanced by texturing the cell surface [73]. The NiO can be used as an HTL to replace spiro-OMeTAD, obtaining a reduced parasitic absorption and an improved current. In addition to needing to reach high enough PCEs, near 30% [84], the main obstacle for perovskite/silicon tandems to be mass produced is spin coating halide perovskites on silicon bottom cells, which limits the cell active area.

A possible strategy consists of the so-called "mechanically stacked four terminal tandem devices". [55,101]. Moreover, the different active areas between the perovskite upper cell and the bottom heterojunction c-Si cell led to complex fabrication methods in two-terminal PSTSC, and the electrical features of the TSCs can be reduced [59,65,102]. Slot-die coating has been proposed to improve scalability of the building process [103]. A high efficiency material suitable for making an ink for the slot-die technique is the triple-halide perovskite with optimized bandgaps [71]. Usually, the film coating requires to be annealed to improve its quality; this step of the process is important, and not only for the transport properties. Indeed, it has been observed that the bandgap linearly decreases with annealing temperature increments, changing from 1.68 eV at 100 °C to 1.66 eV at 170 °C annealing. Despite the fact that annealing the sample at 150 °C gives the intermediate bandgap of 1.67 eV, the quasi-Fermi level splitting shows the highest value among the annealing conditions at 1.26 eV, indicating that the annealing procedure leads to low non-radiative recombination.

A longer charge lifetime has also been observed for the 150 °C annealing condition and has been used to develop the best slot-die coated single-junction solar, reaching FF values of about 78%. A spin coated halide perovskite of the same composition can reach FFs above 81% [71]. The worst behavior of the cells obtained can be explained by comparing the time-resolved photoluminescence of a film obtained by spin coating with that obtained by the slot die. The former has a lifetime of about 3 µs while the latter only has a lifetime of 0.7 µs, probably due to the different crystalline morphology [103]. The best tandem solar cells made with spin coating perform better than the best tandem solar cells made with a slot die, but the latter have demonstrated good industrial scalability, so they represent a major achievement in silicon/perovskite tandem technology [104,105].

5. Perovskite/CIGS Solar Cells

Perovskite/CIGS tandem solar cells have some advantages over silicon-based solar cells, despite having a lower PCE. They are an effective, adaptable, sustainable, and lightweight option since they can be built on flexible substrates [106,107] and, like all thin film technologies, have a substantially smaller carbon footprint per kWh produced. A scheme of a device and its energy levels are shown in Figure 7. Thanks to their radiation hardness [108], perovskite/CIGS tandems may offer a high energy yield option for space applications. Recently, studies by Brown et al. [109] indicated that hybrid perovskite-based solar cells can work reliably in the harsh environments found on Mars, Jupiter, or Saturn. These cells can be produced and interconnected directly on large, ultra-thin polyimide sheets [110,111], and, therefore, they have a future in a wide range of ground and space applications.

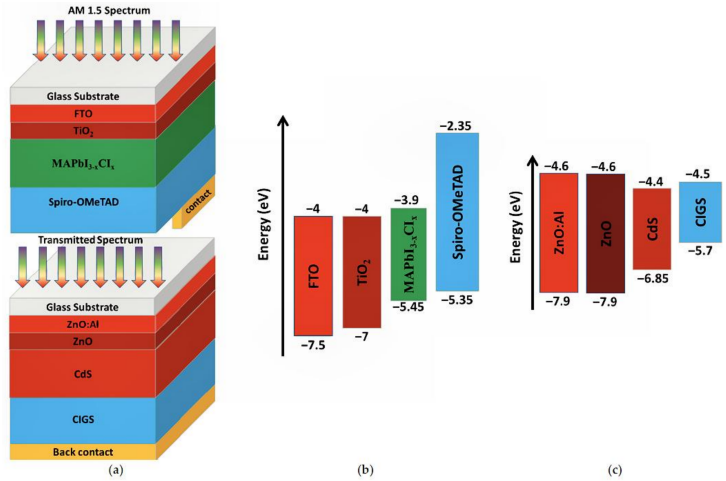

Figure 7. (**a**) Scheme of a perovskite/CIGS tandem device configuration and the corresponding energy levels of the (**b**) upper and (**c**) lower cells. (Figures reprinted from Salah et al. [107], Copyright (2023) with permission of Energies, MDPI).

The first perovskite/CIGS monolithic multijunction solar cell was demonstrated by Tordov et al. [112] in 2015. They proposed a multilayer structure consisting of a transparent conducting electrode (TCE)/PCBM/perovskite/poly(3,4-ethylenedioxythiophene)polystyrenesulfonate (PEDOT:PSS)/ITO/CdS/CIGS/$MoSi_3N_4$/glass. The 30 nm thick ITO layer was deposited directly on the CdS and worked as a recombination layer. The key part of the work was the proposed bandgap engineering method that allowed tuning the $MAPb(I_xBr_{1-x})_3$ perovskite bandgap between 1.65 and 1.75 eV. The most efficient device was obtained with a perovskite layer with a bandgap of 1.72 eV, which reached a PCE of 10.98%. The efficiency was limited by the parasitic absorption of the top electrode that was built by a Ca (10–15 nm)/bathocuproine (BCP) (≈5 nm) film, where Ca was working as a diffusion barrier and the BCP was playing the role of an n-selective layer. The problem of the transparent electrode has been approached by many researchers and still today it is not solved.

Guchhait et al. [113] compared Ag and MoO_x as the buffer layer for ITO deposition in the upper electrode. Compared with the Ag, the use of MoO_x led to a significant dropping of the FF to be ascribed to the oxide lower conductivity. Even though the bandgaps of Si and CIGS were very close to one another and the theoretical limit of PCE should have been nearly the same, the obtained PCE was far from the perovskite/silicon tandem. Simulations highlight that the design can greatly improve the performance. Indeed, a suitable model both for charge transport and optical allows a fine tuning of the absorber, ETL, and HTL thicknesses, and different doping concentrations of perovskite and HTL layers, demonstrating that an efficiency of up to 30% can be achieved [114]. In 2022, Jošt et al. [115] certified a record PCE of 24.2% obtained by a monolithic perovskite/CIGS tandem device. The proposed cell was grown onto a molybdenum-coated glass substrate and consisted of a p–i–n top cell directly deposited on a CIGS bottom cell. The absorber quality of the latter was improved with rubidium fluoride post deposition [116]. To achieve the P–N junction, the cell was completed with a CdS layer and an aluminum-doped ZnO film, which worked, in the tandem design, both as a window layer and as a recombination layer. A wide 1.68 eV bandgap perovskite with a precursor composition of $Cs_{0.05}(MA_{0.23}FA_{0.77})Pb_{1.1}(I_{0.77}Br_{0.23})_3$ [117] and PEAI (phenethylammonium iodide) additive [118] was spin casted next. The structure design then included a 1 nm thermally evaporated LiF thin film and 20 nm of C60 [71]. The cell was completed by an electronic selective contact obtained by depositing 20 nm of SnO_2 and a 95 nm IZO buffer layer with the function of transparent conductive oxide. Finally, a 110 nm layer of LiF acted as an anti-reflection coating. The use of a sputtered ITO electrode in the top semitransparent cell was also approached in a 4T structure proposed by Nakamura et al. in the same year [119].

Usually, a MoO_x buffer layer is interposed below the electrode to avoid damage of the underlying HTL from bombardment by high-energy particles during sputtering of the top electrode of n–i–p type devices [41]. Nevertheless, a MoO_x layer reduces the transmittance in the near infrared, and the heating during the sputtering reduces its durability [33]. They proposed a buffer-free semitransparent top cell, demonstrating no relevant effect of ion bombardment during ITO sputtering on largely used spiro-OMeTAD, whereas the PCE of a 4T 1 cm^2 device was improved by up to 26.2% owing to the better band alignment caused by oxidation of the HTL. An interesting aspect of perovskite/CIGS technology is that it is possible to realize high-efficiency PV devices at low cost by high-efficiency roll-to-roll machining on flexible substrates that ensure industrial scalability. In 2017, using a low-temperature vacuum-based technique, Pisoni et al. [120] grew a NIR-transparent PSC on top of the commercial CIGS encapsulation front sheets, demonstrating the first flexible perovskite/CIGS 4T tandem solar cell with a combined efficiency of 18.2%. They also improved the cell performance by up to 19.65%, adopting a multistage grown process to deposit the perovskite [121]. The scalability and possible commercialization of these solar cells are also closely linked to the possibility of realizing devices of dimensions at least comparable with those of silicon technology. As the PCE decreases as the surface of the cells increases [122], currently the dimensions of the tandem perovskite/CIGS solar cells are of the order of cm^2 [106], and decidedly are not suitable for commercialization. In 2017, a scalable 4T solar module with a perovskite/CIGS structure was proposed by Paetzold et al. [123]. They demonstrated a 3.76 cm^2 device consisting of two thin-film solar module submodules interconnected using stripes of 7 mm × 2.86 mm ($CH_3NH_3PbI_3$ top solar module) and 4 mm × 4.7 mm (CIGS bottom solar module), each at least 20 mm long. The module performed a PCE of 17.8%, which was the sum of the 12% PCE of the semitransparent $CH_3NH_3PbI_3$ top solar module and the 5.8% PCE measured for the CIGS bottom solar module (filtered by the $CH_3NH_3PbI_3$ top module) [123]. Nanosecond pulse laser scribing technology and lift off have been used to fabricate perovskite modules, with the aim of obtaining a higher geometric filling factor but limiting as possible the heat-affected zone [124]. Using an all-laser scribed interconnection approach, Kothandaraman et al. [106] built the interconnection of the mini modules on soft flexible substrate, demonstrating a PCE of 18.4% on an aperture area of 2.03 cm^2.

6. Perovskite/Perovskite Tandem Solar Cells

The realization of the perovskite/perovskite tandem solar cell (PPTSC) is an alternative approach to achieve a high PCE with some advantages, such as simple bandgap tuning of perovskite absorbers, cost-effective and low-temperature monolithic production processes for both the sub-cells, and use of inexpensive precursor materials on flexible substrates [66,97,125,126].

Interestingly, a detailed balance theory has demonstrated that the PCE of TSC may go beyond 45% using optimum material bandgaps (~1.1 eV and ~1.73 eV) [10,127,128], allowing the prediction of a great advantage in using a monolithic perovskite-based design, as the bandgap of these materials is easily tunable. A key challenge is to save the quality of the lower cell while processing the upper cell. As for SHJ and CIGS, perovskite bottom cells also require processing temperatures below 200 °C, and therefore all contact layers need to be processed at low temperatures. This has been realized in both n–i–p [126,129–131] and p–i–n [125,132–136] sub-cell architectures, the latter one being more frequently used because it allows a better efficiency to be obtained. The first example of PPTSC used two analogue sub-cells with similar absorbing materials: the MA lead iodide ($MAPbI_3$) and the $MAPbBr_3$. They were connected with a 2 µm thick doped HTL by a lamination procedure [137]. Despite the demonstration of a V_{OC} as high as 2.2 V (that corresponds to the sum of the two sub-cell V_{OC}), the PCE was limited due to the spectral properties of the absorbing layers, which in turn greatly reduced the overall attainable current density. The PCE was further reduced by the low conductivity of the HTL layer due to its thickness. The HTL transport properties have been improved by Li-TFSI additives that act as hole

conductors such as quasi-solid electrolytes because the additives provide Li/Li^+ redox shuttle [138]. Selecting proper materials with complementary bandgaps, Lin et al. [132] built a maximum PCE of 24.8% by monolithically fabricating all-perovskite PPTSC. They used 1.22 eV and 1.77 eV bandgap perovskites as bottom and top sub-cells, respectively, demonstrating the perovskite flexibility in terms of bandgap [132]. A schematic cross-section of the proposed planar PPTSC is shown in Figure 8. The front contact ETL consists of 50 nm Al-doped ZnO (AZO) followed by a perovskite absorber layer. A double layer of NiO/AZO is utilized as an HTL, where a very thin NiO is used with a 50 nm thick AZO film. Furthermore, the combined NiO/AZO layer works as a tunneling junction, facilitating efficient charge carrier transportation [139–142]. Finally, a 100 nm Al is used as a back reflector. Concerning the absorbing layer, the top cell consists of a wide bandgap (Eg~1.72 eV) $Cs_yFA_{1-y}Pb(I_xBr_{1-x})_3$ perovskite with a composition ratio of 0.1, while a low bandgap (Eg~1.16 eV) $MASn_xPb_{1-x}I_3$ perovskite with a composition factor of 0.85 is utilized as a bottom cell. As the overall efficiency strongly depends on the electrodes' transport qualities, some effort has been devoted to improving the ETL layer also. This latter usually consists of a mesoporous–titanium dioxide thin film, which, however, can allow non-radiative recombination at the ETL perovskite interface, worsening the performance. It has been demonstrated that a thin layer of polyacrylic-acid-stabilized tin (IV) oxide quantum dots (paa-QD-SnO_2) on the compact titanium dioxide enhances light capture and widely suppresses nonradiative recombination. Using paa-QD-SnO_2 as the electron-selective contact enabled PSCs (0.08 cm^2) with a PCE of 25.7% (certified 25.4%) and allowed an increase of the PSC areas. Namely, areas of 1.20 and 64 cm^2 were obtained with PCEs of 23.3, 21.7 and 20.6%, respectively [30].

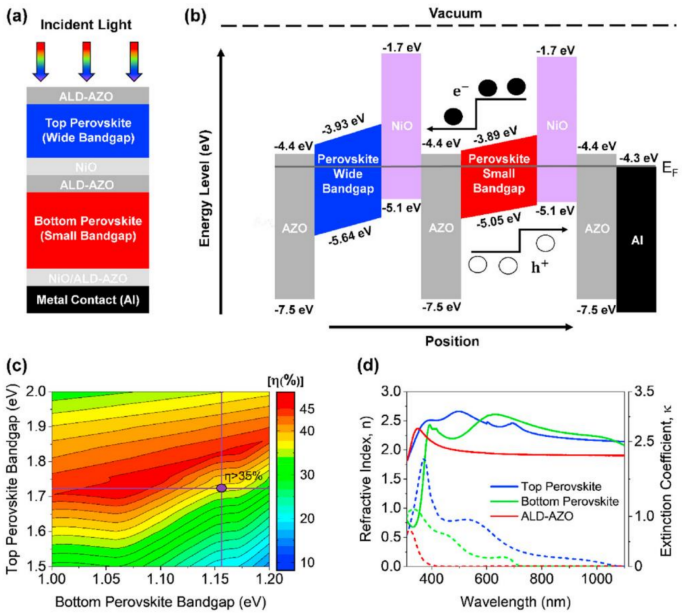

Figure 8. (**a**) Scheme and (**b**) corresponding energy levels of the planar perovskite/perovskite tandem solar cell. (**c**) Theoretical upper energy conversion efficiency (ECE) limit of two-terminal (2T) monolithic. (**d**) Refractive index and extinction coefficient curves (solid and dashed curves, respectively) of large and narrow bandgap perovskites along with ALD Al-doped ZnO (AZO). (Figures reprinted from Hossain et al. [139], copyright (2023) with permission of Nano Energy).

Another possible strategy proposed to improve the ETL transport properties consists of introducing iodine-doped g-C_3N_4 (ICN) as an additive via a glass-assisted annealing route into $ZnTiO_3$. The ETL thus obtained has a better crystalline quality and a more adequate alignment of energy levels, and, when used, results in a better PCE [143]. Some authors have focused their attention on the carrier diffusion length of the perovskite layer that should be many times the absorber thickness to guarantee good PV performance and

sufficient charge transport in PSCs [144,145]. Unfortunately, diffusion length is mainly limited by grain surface traps, the number of which is very large compared with the number of traps distributed within the grain [146–149].

Hence, grain surface passivation has been proposed as a promising route to improve carrier diffusion and PCE [150–152], as this strategy overcomes the limits due to the diffusion length, allowing a thicker absorption layer (>1 µm) that, in turn, improves the photons catching. 4-Trifluoromethyl-phenylammonium (CF3-PA) has been used as a strong perovskite surface passivator capable of increasing the diffusion length by up to 5 µm and skyrocketing the PCE to over 26%.CF3-PA passivated tandem devices maintained 90% of their initial PCE after 600 h of operation at the maximum power point under 1 sun illumination in ambient conditions, exhibiting better performance when compared with unpassivated devices [153]. Another well-known problem of PPTSC concerns the low V_{OC}, since Br concentrations higher than 20% lead to an increase in the density of traps. In addition, photoinduced halide segregation effects and poor energy alignment with the charge transport layers are possible [154,155]. Finally, the interface with the charge transport layers can give rise to localized states within the perovskite bandgap, which, acting as recombination centers, reduce the quantum yield [156–158]. The origin of this phenomenon has been attributed to several causes including band misalignment [158], energy-level pinning [154], and halide migration from the perovskite into the transport layer [159]. A typical example of the above issue is the case high performance PPTSC using fullerene ETL that is considered one of the worst offenders regarding the induction of trap states.

Surface passivation using organic phenethylammonium iodide (PEAI) halide salt [160] or butylammonium iodide (BA) [161] and 1,3-propane-diammonium iodide [162] is a possible strategy proposed to improve PCE by reducing trap states. Recently, bifacial solar cells have attracted the attention of researchers as they can achieve a higher PCE since they can absorb reflected and scattered light (albedo) that achieves the cell's back-surface (Figure 9). The main difference consists of using or not using a reflecting layer as the bottom electrode. The possibility of making semitransparent PPTSC represents a great opportunity for the development and application of high-efficiency bifacial cells. In fact, the tandem cells, which can be manufactured using the thin film technology, are excellent candidates because they simultaneously offer a high PCE and a structure that easily allows the lower cell to integrate transparent bottom electrodes, making the cell active also towards the light that comes from below. According to numerical simulation, the benefits of tandem architecture and bifacial design can be inherited by bifacial tandem cells, allowing for higher thermodynamic efficiency than monofacial tandems and single-junction designs [163,164].

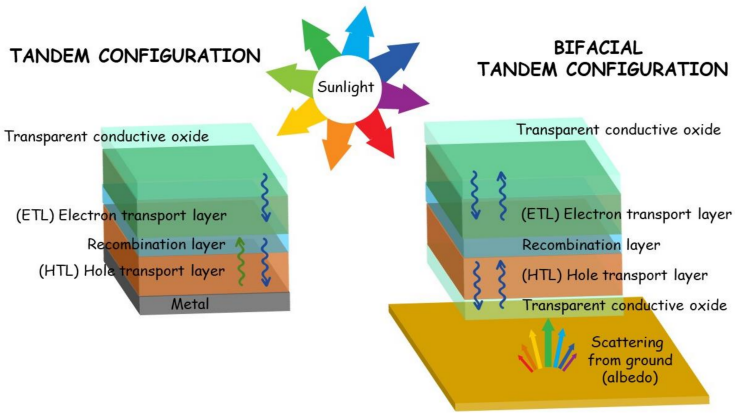

Figure 9. Scheme of tandem and bifacial tandem configurations.

In 2022, Li and co-workers [165] developed the first bifacial all-perovskite tandem by using TCO as a rear electrode, starting from an already well known monofacial configuration. The flexibility in designing the perovskite bandgap allowed optimization of the PCE

under different realistic illumination and albedo conditions, a PCE > 25% under AM1.5G 1 sun illumination to be obtained. Moreover, in field tests, it is possible to gain a power density as high as 26 mW·cm^{-2} [166]. The cell architecture also needs to be investigated; indeed, the thickness of an absorber in a 2T bifacial tandem configuration strongly depends upon the magnitude of albedo due to the current-matching constraint between the sub-cells, while the 4T configuration can work better for a wide range of albedo (Figure 10) [167].

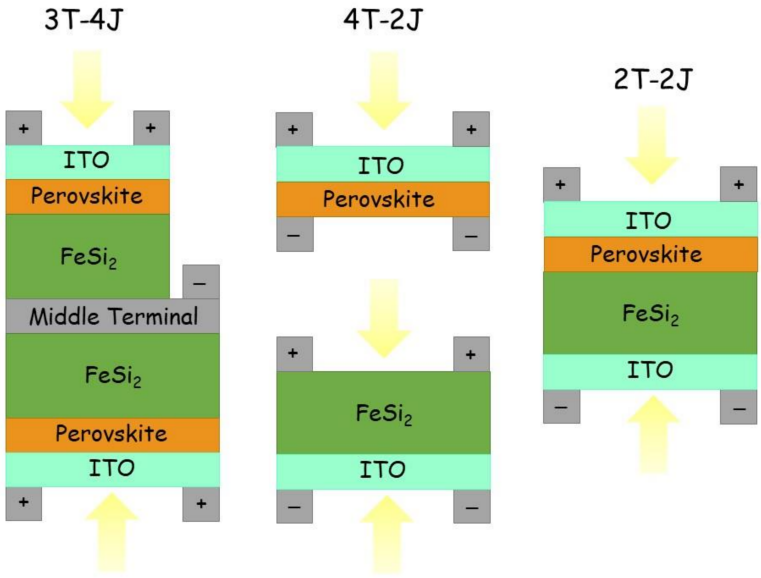

Figure 10. Scheme of 3T-4J, 4T-2J, and 2T-2J configurations of bifacial tandem solar cells.

7. Conclusions

Over the past few decades, interest in perovskite materials for green energy generation has grown rapidly. In 2009, the first photovoltaic cell reported in the literature involved the self-assembly process of organic–inorganic lead halide perovskite nanocrystalline particles, $CH_3NH_3PbBr_3$ and $CH_3NH_3PbI_3$, on a TiO_2 n-type semiconductor. These simple layered structures can achieve a conversion efficiency as high as 3.8% and a photovoltage of 0.96 V. They represent the milestone in the use of perovskites in photovoltaic applications. Continuous improvements in design, materials, and optimization of the device architecture allow the achievement of important goals. (i) An efficiency approaching 29% was obtained in PSTSC, optimizing the HTL. (ii) In 2015, CIGS substituted for the Si in the PV tandem cells. Although the bandgaps of Si and CIGS are very close to each other, a PCE of 24.2% was achieved only in 2022, after an accurate optimization of the absorber, ETL, and HTL thicknesses, and different doping concentrations of perovskite and HTL layers. (iii) Finally, the realization of PPTSC allowed a PCE value of 26% to be reached, introducing the CF3-PA as a perovskite surface passivator to increase the carrier diffusion length.

The main achievements and advantages summarized here suggest that the perovskite-based tandem solar cell could be an efficient system to exploit the solar light to produce "green energy". However, many issues still represent open questions for the effective use of this technology. Issues around industrial scalability and production processes are two common factors for all described perovskite-based tandem solar cells. The interesting performances reported in the literature have been demonstrated for solar cells with an area of about 1 cm^2 (the area of a single Si-based solar cell is about 20 cm^2). A larger area of the device, together with mass production and low costs, represents important challenges in the PV research field, especially for the optimization of the building process. In addition, although the rapid optimization of perovskite-based tandem solar cells allows achievement of high efficiency in a very short time, perovskites are characterized by short lifetimes, not compatible with the current commercial technology. The prolonged exposure to the sun activates a deterioration process of the material, which affects the durability and the

efficiency of the device. The first approach to reduce the deterioration, i.e., coating the surface with an organic ion layer with a mixing of positive and negative ions, has partly solved the issue, allowing 2000 h of operation to be achieved.

Currently, further investigations and studies are needed to open the commercial market, but the obtained optimal performance represents a good reason to continue the research activity in the incorporation of perovskite in tandem solar cells.

Funding: This research received no external funding.

Data Availability Statement: Not applicable.

Conflicts of Interest: The authors declare no conflict of interest.

Abbreviations & Nomenclature

AM	Air Mass
ALD	Atomic Layer Deposition
AZO	Aluminum-doped Zinc Oxide
BA	Butylammonium iodide
a-Si	Amorphous silicon
a-Si:H	Hydrogenated amorphous silicon
c-Si	Crystalline silicon
CdTe	Cadmium-Telluride
CF3-PA	4-Trifluoromethyl-phenylammonium
CIGS	Copper Indium Gallium Selenide
ETL	Electron Transporting Layer
FA	Formamidinium
FF	Fill Factor
FTO	Fluorine-doped Tin Oxide
GaAs	Gallium Arsenide
GaInP	Gallium Indium Phosphate
GaInAs	Gallium Indium Arsenide
HIT	Heterojunction with Intrinsic Thin-layer
HTL	Hole Transporting Layer
IBC	Interdigitated Back Contact
ICN	Iodine-doped g-C_3N_4
IRENA	International Renewable Energy Agency
ITO	Indium Tin Oxide
IZO	Indium Zinc Oxide
J_{SC}	Short-circuit current density
MA	Methylammonium
NWs	Nanowires
PCBM	[6,6]-Phenyl-C61-butyric acid methyl ester
PCE	Power Conversion Efficiency
PDMS	Polydimethylsiloxane
PEAI	Phenethylammonium iodide
PECVD	Plasma-enhanced chemical vapor deposition
PEIE	Polyethylenimine
PET	Polyethylene Terephthalate
PPTSC	Perovskite/Perovskite Tandem Solar Cell
PSTSCs	Perovskite-Silicon Tandem Solar Cells
PV	Photovoltaics
QD	Quantum Dots
QW	Quantum Well
SHJ	Silicon heterojunction
TCO	Transparent Conductive Oxides
V_{OC}	Open-circuit voltage

References

1. Nayak, P.K.; Mahesh, S.; Snaith, H.J.; Cahen, D. Photovoltaic solar cell technologies: Analysis of the state of the art. *Nat. Rev. Mater.* **2019**, *4*, 269–285. [CrossRef]
2. Wilson, G.M.; Al-Jassim, M.; Metzger, W.K.; Glunz, S.W.; Verlinden, P.; Xiong, G.; Mansfield, L.M.; Stanbery, B.J.; Zhu, K.; Yan, Y. The 2020 photovoltaic technologies roadmap. *J. Phys. D Appl. Phys.* **2020**, *53*, 493001. [CrossRef]
3. Green, M. Limits on the open-circuit voltage and efficiency of silicon solar cells imposed by intrinsic auger processes. *IEEE Trans. Electron Devices* **1982**, *31*, 671–678. [CrossRef]
4. Swanson, R.M. Approaching the 29% limit efficiency of silicon solar cells. In Proceedings of the Conference Record of the Thirty-First IEEE Photovoltaic Specialists, Lake Buena Vista, FL, USA, 3–7 January 2005; pp. 889–894.
5. Richter, A.; Hermle, M.; Glunz, S.W. Reassessment of the limiting efficiency. *IEEE J. Photovolt.* **2013**, *3*, 1184–1191. [CrossRef]
6. Green, M.A. Limiting photovoltaic efficiency under new ASTM International G173-based reference spectra. *Prog. Photovolt.* **2012**, *20*, 954–959. [CrossRef]
7. Okuda, K.; Okamoto, H.; Hamakawa, Y. Amorphous Si/polycrystalline Si stacked solar cell having more than 12% conversion efficiency. *Jpn. J. Appl. Phys.* **1983**, *9*, 1605–1607. [CrossRef]
8. Tanaka, M.; Taguchi, M.; Matsuyama, T.; Sawada, T.; Tsuda, S.; Nakano, S.; Hanafusa, H.; Kuwano, Y. Development of New a-Si/c-Si Heterojunction Solar Cells: ACJ-HIT (Artificially Constructed Junction-Heterojunction with Intrinsic Thin-Layer. *Jpn. J. Appl. Phys.* **1992**, *31*, 3518. [CrossRef]
9. Green, M.A.; Hishikawa, Y.; Warta, W.; Dunlop, E.D.; Levi, D.H.; Hohl-Ebinger, J.; Ho-Baillie, A. Solar cell efficiency tables (version 50). *Prog. Photovolt. Res. Appl.* **2017**, *25*, 668–676. [CrossRef]
10. Shockley, W.; Queisser, H.J. Detailed balance limit of efficiency of p-n junction solar cells. *J. Appl. Phys.* **1961**, *32*, 510–519. [CrossRef]
11. Geisz, J.F.; France, R.M.; Schulte, K.L.; Steiner, M.A.; Norman, A.G.; Guthrey, H.L.; Young, M.R.; Song, T.; Moriarty, T. Six-junction III–V solar cells with 47.1% conversion efficiency under 143 Suns. *Nat. Energy* **2020**, *5*, 326–335. [CrossRef]
12. France, R.M.; Geisz, J.F.; Song, T.; Olavarria, W.; Young, M.; Kibbler, A.; Steiner, M.A. Triple-junction solar cells with 39.5% terrestrial and 34.2% space efficiency enabled by thick quantum well superlattices. *Joule* **2022**, *6*, 1121–1135. [CrossRef]
13. Mailoa, J.P.; Bailie, C.D.; Johlin, E.C.; Hoke, E.T.; Akey, A.J.; Nguyen, W.H.; McGehee, M.D.; Buonassisi, T. A 2-terminal perovskite/silicon multijunction solar cell enabled by a silicon tunnel junction. *Appl. Phys. Lett.* **2015**, *106*, 121105. [CrossRef]
14. Guo, F.; Li, N.; Radmilović, V.V.; Radmilović, V.R.; Turbiez, M.; Spiecker, E.; Forbericha, K.; Brabec, C.J. Fully printed organic tandem solar cells using solution-processed silver nanowires and opaque silver as charge collecting electrodes. *Energy Environ. Sci.* **2015**, *8*, 1690–1697. [CrossRef]
15. Tyagi, B.; Lee, H.B.; Kumar, N.; Jin, W.Y.; Ko, K.J.; Ovhal, M.M.; Sahani, R.; Chung, H.J.; Seo, J.; Kang, J.W. High-performance, large-area semitransparent and tandem perovskite solar cells featuring highly scalable a-ITO/Ag mesh 3D top electrodes. *Nano Energy* **2022**, *95*, 106978. [CrossRef]
16. Lamanna, E.; Matteocci, F.; Calabrò, E.; Serenelli, L.; Salza, E.; Martini, L.; Menchini, F.; Izzi, M.; Agresti, A.; Pescetelli, S.; et al. Mechanically Stacked, Two-Terminal Graphene-Based Perovskite/Silicon Tandem Solar Cell with Efficiency over 26%. *Joule* **2020**, *4*, 865–881. [CrossRef]
17. Cheng, Y.; Ding, L. Perovskite/Si tandem solar cells: Fundamentals, advances, challenges, and novel applications. *SusMat* **2021**, *1*, 324–344. [CrossRef]
18. Assirey, E.A.R. Perovskite synthesis, properties and their related biochemical and industrial application. *Saudi Pharm. J.* **2019**, *27*, 817–829. [CrossRef]
19. Wei, Q.; Ning, Z. Chiral Perovskite Spin-Optoelectronics and Spintronics: Toward Judicious Design and Application. *ACS Mater. Lett.* **2021**, *9*, 1266–1275. [CrossRef]
20. Hwang, J.; Rao, R.R.; Giordano, L.; Katayama, Y.; Shao-Horn, Y. Perovskites in catalysis and electrocatalysis. *Science* **2017**, *358*, 751–756. [CrossRef]
21. Kojima, A.; Teshima, K.; Shirai, Y.; Miyasaka, T. Organometal Halide Perovskites as Visible-Light Sensitizers for Photovoltaic. *J. Chem. Soc. Chem. Commun.* **2009**, *131*, 6050–6051. [CrossRef]
22. Yoo, J.J.; Seo, G.; Chua, M.R.; Park, T.G.; Lu, Y.; Rotermung, F.; Kim, Y.K.; Moon, C.S.; Jeon, N.J.; Correa-Baena, J.P.; et al. Efficient perovskite solar cells via improved carrier management. *Nature* **2021**, *590*, 587–594. [CrossRef]
23. Kim, G.; Kim, D.S. Development of perovskite solar cells with >25% conversion efficiency. *Joule* **2021**, *5*, 1033–1035. [CrossRef]
24. Lee, M.M.; Teuscher, J.; Miyasaka, T.; Murakami, T.N.; Snaith, H.J. Efficient Hybrid Solar Cells Based on Meso-Superstructured Organometal Halide Perovskites. *Science* **2012**, *338*, 643–647. [CrossRef]
25. Park, M.; Kornienko, N.; Reyes-Lillo, S.E.; Lai, M.; Neaton, J.B.; Yang, P.; Mathies, R.A. Critical Role of Methylammonium Librational Motion in Methylammonium Lead Iodide ($CH_3NH_3PbI_3$) Perovskite Photochemistry. *Nano Lett.* **2017**, *17*, 4151–4157. [CrossRef]
26. Shi, E.; Yuan, B.; Shiring, S.B.; Gao, Y.; Guo, Y.; Su, C.; Lai, M.; Yang, P.; Kong, J.; Savoie, B.M.; et al. Two-dimensional halide perovskite lateral epitaxial heterostructures. *Nature* **2020**, *580*, 614–620. [CrossRef]
27. He, Q.; Worku, M.; Liu, H.; Lochner, E.; Robb, A.J.; Lteif, S.; Winfred, J.S.; Hanson, K.; Schlenoff, J.B.; Kim, B.J.; et al. Highly Efficient and Stable Perovskite Solar Cells Enabled by Low-Cost Industrial Organic Pigment Coating. *Angew. Chem. Int.* **2021**, *60*, 2485–2492. [CrossRef]

28. Pham, N.D.; Singh, A.; Chen, W.; Hoang, M.T.; Yang, Y.; Wang, X.; Wolff, A.; Wen, X.; Jia, B.; Sonar, P.; et al. Self-assembled carbon dot-wrapped perovskites enable light trapping and defect passivation for efficient and stable perovskite solar cells. *J. Mater. Chem. A* **2021**, *9*, 7508–7521. [CrossRef]
29. Kim, D.; Jung, H.J.; Park, I.J.; Larson, B.W.; Dunfield, S.P.; Xiao, C.; Kim, J.; Tong, J.; Boonmongkolras, P.; Ji, S.G.; et al. Efficient, stable silicon tandem cells enabled by anion-engineered wide-bandgap perovskites. *Science* **2020**, *368*, 155–160. [CrossRef]
30. Xiong, S.; Hou, Z.; Zou, S.; Lu, X.; Yang, J.; Hao, T.; Zhou, Z.; Xu, J.; Zeng, Y.; Xiao, W.; et al. Direct Observation on p- to n-Type Transformation of Perovskite Surface Region during Defect Passivation Driving High Photovoltaic Efficiency. *Joule* **2021**, *5*, 467–480. [CrossRef]
31. Kim, M.; Jeong, J.; Lu, H.; Lee, T.K.; Eickemeyer, F.T.; Liu, Y.; Choi, I.W.; Choi, S.J.; Jo, Y.; Kim, H.B.; et al. Conformal quantum dot–SnO_2 layers as electron transporters for efficient perovskite solar cells. *Science* **2022**, *375*, 302–306. [CrossRef]
32. Tan, S.; Huang, T.; Yavuz, I.; Wang, R.; Yoon, T.W.; Xu, M.; Xing, Q.; Park, K.; Lee, D.-K.; Chen, C.-H.; et al. Stability-limiting heterointerfaces of perovskite photovoltaics. *Nature* **2022**, *605*, 268–273. [CrossRef] [PubMed]
33. Fu, F.; Feurer, T.; Jäger, T.; Avancini, E.; Bissig, B.; Yoon, S.; Buecheler, S.; Tiwari, A.N. Low-temperature-processed efficient semi-transparent planar perovskite solar cells for bifacial and tandem applications. *Nat. Commun.* **2015**, *6*, 8932. [CrossRef] [PubMed]
34. Green, M.A.; Dunlop, E.D.; Hohl-Ebinger, J.; Yoshita, M.; Kopidakis, N.; Hao, X. Solar cell efficiency tables (Version 58). *Prog. Photovolt. Res. Appl.* **2021**, *29*, 657–667. [CrossRef]
35. Mao, L.; Yang, T.; Zhang, H.; Shi, J.; Hu, Y.; Zeng, P.; Li, F.; Gong, J.; Fang, X.; Park, K.; et al. Fully Textured, Production-Line Compatible Monolithic Perovskite/Silicon Tandem Solar Cells Approaching 29% Efficiency. *Adv. Mater.* **2022**, *34*, 2206193. [CrossRef] [PubMed]
36. Kopecek, R.; Koduvelikulathu, L.J.; Tune, D.; Kirk, D.; Case, C.; Rienacker, M.; Schulte-Huxel, H.; Warren, E.L.; Tamboli, A.; Peibst, R.; et al. Tandem PV: A review of c-Si-based tandem technology and what is needed to bring it into production. *PV Int.* **2020**, *45*, 40–52.
37. Bailie, C.D.; Christoforo, M.G.; Mailoa, J.P.; Bowring, A.R.; Unger, E.L.; Nguyen, W.H.; Burschka, J.; Pellet, N.; Lee, J.Z.; Gratzel, M.; et al. Semi-transparent perovskite solar cells for tandems with silicon and CIGS. *Energy Environ. Sci.* **2015**, *8*, 956–963. [CrossRef]
38. Kato, Y.; Ono, L.K.; Lee, M.V.; Wang, S.; Raga, S.R.; Qi, Y. Silver Iodide Formation in Methyl Ammonium Lead Iodide Perovskite Solar Cells with Silver Top Electrodes. *Adv. Mater. Interfaces* **2015**, *2*, 1500195. [CrossRef]
39. Liu, D.; Gangishetty, M.K.; Kelly, T.L. Effect of $CH_3NH_3PbI_3$ thickness on device efficiency in planar heterojunction perovskite solar cells. *Mater. Chem. A* **2014**, *2*, 19873–19881. [CrossRef]
40. Löper, P.; Moon, S.-J.; De Nicolas, S.M.; Niesen, B.; Ledinsky, M.; Nicolay, S.; Bailat, J.; Yum, J.-H.; De Wolf, S.; Ballif, C. Organic–inorganic halide perovskite/crystalline silicon four-terminal tandem solar cells. *Phys. Chem. Chem. Phys.* **2015**, *17*, 1619–1629. [CrossRef]
41. Duong, T.; Lal, N.; Grant, D.; Jacobs, D.; Zheng, P.; Rahman, S.; Shen, H.; Stocks, M.; Blakers, A.; Weber, K.; et al. Semitransparent Perovskite Solar Cell with Sputtered Front and Rear Electrodes for a Four-Terminal Tandem. *IEEE J. Photovolt.* **2016**, *6*, 679–687. [CrossRef]
42. Li, X.; Bi, D.; Yi, C.; Décoppet, J.D.; Luo, J.; Zakeeruddin, S.M.; Hagfeldt, A.; Grätzel, M. A vacuum flash-assisted solution process for high-efficiency large-area perovskite solar cells. *Science* **2016**, *353*, 58–62. [CrossRef]
43. Burschka, J.; Pellet, N.; Moon, S.J.; Baker, R.H.; Gao, P.; Nazeeruddin, M.K.; Gratzel, M. Sequential deposition as a route to high-performance perovskite-sensitized solar cells. *Nature* **2013**, *499*, 316–319. [CrossRef]
44. Peng, J.; Duong, T.; Zhou, X.; Shen, H.; Wu, Y.; Mulmudi, H.K.; Wan, Y.; Zhong, D.; Li, J.; Tsuzuki, T.; et al. Efficient Indium-Doped TiO_x Electron Transport Layers for High-Performance Perovskite Solar Cells and Perovskite-Silicon Tandems. *Adv. Energy Mater.* **2017**, *7*, 1601768. [CrossRef]
45. Coutts, T.J.; Emery, K.A.; Ward, J.S. Modeled performance of polycrystalline thin-film tandem solar cells. *Prog. Photovolt.* **2002**, *10*, 195–203. [CrossRef]
46. Filipič, M.; Löper, P.; Niesen, B.; De, W.S.; Krč, J.; Ballif, C.; Topič, M. $CH_3NH_3PbI_3$ perovskite/silicon tandem solar cells: Characterization based optical simulations. *Opt. Express* **2015**, *23*, A263–A278. [CrossRef]
47. Futscher, M.H.; Ehrler, B. Efficiency Limit of Perovskite/Si Tandem Solar Cells. *ACS Energy Lett.* **2016**, *1*, 863–868. [CrossRef]
48. Zhang, Y.; Liu, Y.; Yang, Z.; Liu, S. High-quality perovskite $MAPbI_3$ single crystals for broad-spectrum and rapid response integrate photodetector. *J. Energy Chem.* **2018**, *27*, 722–727. [CrossRef]
49. Yu, Z.S.; Leilaeioun, M.; Holman, Z. Selecting tandem partners for silicon solar cells. *Nat. Energy* **2016**, *1*, 16137. [CrossRef]
50. Hoke, E.T.; Slotcavage, D.J.; Dohner, E.R.; Bowring, A.R.; Karunadasa, H.I.; Mcgehee, M.D. Reversible photo-induced trap formation in mixed-halide hybrid perovskites for photovoltaics. *Chem. Sci.* **2015**, *6*, 613–617. [CrossRef]
51. Slotcavage, D.J.; Karunadasa, H.I.; McGehee, M.D. Light-Induced Phase Segregation in Halide-Perovskite Absorbers. *ACS Energy Lett.* **2016**, *1*, 1199–1205. [CrossRef]
52. Barker, A.J.; Sadhanala, A.; Deschler, F.; Gandini, M.; Senanayak, S.P. Defect-Assisted Photoinduced Halide Segregation in Mixed-Halide Perovskite Thin Films. *ACS Energy Lett.* **2017**, *2*, 1416–1424. [CrossRef]

53. Bush, K.A.; Frohna, K.; Prasanna, R.; Beal, R.E.; Leijtens, T.; Swifter, S.A.; McGehee, M.D. Compositional Engineering for Efficient Wide Band Gap Perovskites with Improved Stability to Photoinduced Phase Segregation. *ACS Energy Lett.* **2018**, *3*, 428–435. [CrossRef]
54. Tang, X.; Van den Berg, M.; Gu, E.; Horneber, A.; Matt, G.J.; Osvet, A.; Meixner, A.J.; Zhang, D.; Brabec, C.J. Local Observation of Phase Segregation in Mixed-Halide Perovskite. *Nano Lett.* **2018**, *18*, 2172–2178. [CrossRef]
55. Duong, T.; Wu, Y.L.; Shen, H.; Peng, J.; Fu, X.; Jacobs, D.; Wang, E.C.; Kho, T.C.; Fong, K.C.; Stocks, M. Rubidium Multication Perovskite with Optimized Bandgap for Perovskite-Silicon Tandem with over 26% Efficiency. *Adv. Energy Mater.* **2017**, *7*, 1700228. [CrossRef]
56. Chen, B.; Bai, Y.; Yu, Z.; Li, T.; Zheng, X.; Dong, Q.; Shen, L.; Boccard, M.; Gruverman, A.; Holman, Z.; et al. Efficient Semitransparent Perovskite Solar Cells for 23.0%-Efficiency Perovskite/Silicon Four-Terminal Tandem Cells. *Adv. Energy Mater.* **2016**, *6*, 1601128. [CrossRef]
57. Jaysankar, M.; Qiu, W.; Eerden, M.V.; Aernouts, T.; Gehlhaar, R.; Debucquoy, M.; Paetzold, U.W.; Poortmans, J. Four-Terminal Perovskite/Silicon Multijunction Solar Modules. *Adv. Energy Mater.* **2017**, *7*, 1602807. [CrossRef]
58. Liu, Y.; Renna, L.A.; Bag, M.; Page, Z.A.; Kim, P.; Choi, J.; Emrick, T.; Venkataraman, D.; Russell, T.P. High Efficiency Tandem Thin-Perovskite/Polymer Solar Cells with a Graded Recombination Layer. *ACS Appl. Mater. Interfaces* **2016**, *8*, 7070–7076. [CrossRef]
59. Bush, K.A.; Palmstrom, A.F.; Yu, Z.J.; Boccard, M.; Cheacharoen, R.; Mailoa, J.P.; McMeekin, D.P.; Hoye, R.L.; Bailie, C.D.; Leijtens, T.; et al. 23.6%-efficient monolithic perovskite/silicon tandem solar cells with improved stability. *Nat. Energy* **2017**, *2*, 17009. [CrossRef]
60. Masuko, K.; Shigematsu, M.; Hashiguchi, T.; Fujishima, D.; Kai, M.; Yoshimura, N.; Yamaguchi, T.; Ichihashi, Y.; Mishima, T.; Matsubara, N.; et al. Achievement of More Than 25% Conversion Efficiency with Crystalline Silicon Heterojunction Solar Cell. *IEEE J. Photovolt.* **2014**, *4*, 1433–1435. [CrossRef]
61. Mishima, T.; Taguchi, M.; Sakata, H.; Maruyama, E. Development status of high-efficiency HIT solar cells. *Sol. Energy Mater. Sol. Cells* **2011**, *95*, 18–21. [CrossRef]
62. Taguchi, M.; Yano, A.; Tohoda, S.; Matsuyama, K.; Nakamura, Y.; Nishiwaki, T.; Fujita, K.; Maruyama, E. 24.7% Record Efficiency HIT Solar Cell on Thin Silicon Wafer. *IEEE J. Photovolt.* **2014**, *4*, 96–99. [CrossRef]
63. Ying, Z.; Yang, Z.; Zheng, J.; Wei, H.; Chen, L.; Xiao, C.; Sun, J.; Shou, C.; Qin, G.; Sheng, J.; et al. Monolithic perovskite/black-silicon tandems based on tunnel oxide passivated contacts. *Joule* **2022**, *6*, 2644–2661. [CrossRef]
64. Köhnen, E.; Wagner, P.; Lang, F.; Cruz, A.; Li, B.; Rob, M.; Jost, M.; Morales-Vilches, A.B.; Topic, M.; Stolterfoht, M.; et al. 27.9% Efficient Monolithic Perovskite/Silicon Tandem Solar Cells on Industry Compatible Bottom Cells. *Sol. RRL* **2021**, *5*, 2100244. [CrossRef]
65. Sahli, F.; Werner, J.; Kamino, B.A.; Bräuninger, M.; Monnard, R.; Paviet-Salomon, B.; Barraud, L.; Ding, L.; Leon, J.J.D.; Sacchetto, D.; et al. Fully textured monolithic perovskite/silicon tandem solar cells with 25.2% power conversion efficiency. *Nat. Mater.* **2018**, *17*, 820–826. [CrossRef]
66. Hou, Y.; Aydin, E.; De Bastiani, M.; Xiao, C.; Isikgor, F.H.; Xue, D.J.; Chen, B.; Chen, H.; Bahrami, B.; Chowdhury, A.H.; et al. Efficient tandem solar cells with solution-processed perovskite on textured crystalline silicon. *Science* **2020**, *367*, 1135–1140. [CrossRef]
67. EPFL. *New World Records: Perovskite-on-Silicon-Tandem Solar Cells*; Technical Report; Stanford University: Stanford, CA, USA, 2021.
68. Mazzarella, L.; Lin, Y.; Kirner, S.; Morales-Vilches, A.B.; Korte, L.; Albrecht, S.; Crossland, E.; Stannowski, B.; Case, C.; Snaith, H.J.; et al. Infrared Light Management Using a Nanocrystalline Silicon Oxide Interlayer in Monolithic Perovskite/Silicon Heterojunction Tandem Solar Cells with Efficiency above 25%. *Adv. Energy Mater.* **2019**, *9*, 1803241. [CrossRef]
69. Köhnen, E.; Jošt, M.; Belen Morales-Vilches, A.; Tockhorn, P.; Al-Ashouri, A.; Macco, B.; Kegelmann, L.; Korte, L.; Rech, B.; Schlatmann, R.; et al. Highly efficient monolithic perovskite silicon tandem solar cells: Analyzing the influence of current mismatch on device performance. *Science* **2020**, *367*, 1135–1140. [CrossRef]
70. Al-Ashouri, A.; Köhnen, E.; Li, B.; Magomedov, A.; Hempe, H.; Caprioglio, P.; Marquez, J.A.; Morales-Vilches, A.B.; Kasparavicius, E.; Smith, J.A.; et al. Monolithic perovskite/silicon tandem solar cell with >29% efficiency by enhanced hole extraction. *Science* **2020**, *370*, 1300–1309. [CrossRef]
71. Xu, J.; Boyd, C.C.; Yu, Z.J.; Palmstrom, A.F.; Witter, D.J.; Larson, D.J.; France, R.M.; Werner, J.; Harvey, S.P.; Wolf, E.J.; et al. Triple-halide wide–band gap perovskites with suppressed phase segregation for efficient tandems. *Science* **2020**, *367*, 1097–1104. [CrossRef]
72. Schulze, P.S.C.; Bett, A.J.; Bivour, M.; Caprioglio, P.; Gerspacher, F.M.; Kabakli, O.S.; Richter, A.; Stolterfoht, M.; Zhang, Q.; Neher, D.; et al. 25.1% high-efficiency monolithic perovskite silicon tandem solar cell with a high bandgap perovskite absorber. *Sol. RRL* **2020**, *4*, 2000152. [CrossRef]
73. Santbergen, R.; Mishima, R.; Meguro, T.; Hino, M.; Uzu, H.; Blanker, J.; Yamamoto, K.; Zeman, M. Minimizing optical los;ses in monolithic perovskite/c-Si tandem solar cells with a flat top cell. *Opt. Express* **2016**, *24*, A1288–A1299. [CrossRef] [PubMed]
74. Chen, D.; Manley, P.; Tockhorn, P.; Eisenhauer, D.; Köppel, G.; Hammerschmidt, M.; Burger, S.; Albrecht, S.; Becker, C.; Jager, K. Nanophotonic light management for perovskite–silicon tandem solar cells. *J. Photonics Energy* **2018**, *8*, 022601. [CrossRef]

75. Tennyson, E.M.; Frohna, K.; Drake, W.K.; Sahli, F.; Yang, T.C.; Fu, F.; Werner, J.; Chosy, C.; Bowman, A.R.; Doherty, T.A.S.; et al. Multimodal Microscale Imaging of Textured Perovskite–Silicon Tandem Solar Cells. *ACS Energy Lett.* **2021**, *6*, 2293–2304. [CrossRef] [PubMed]
76. Roß, M.; Severin, S.; Stutz, M.B.; Wagner, P.; Köbler, H.; Favin-Leveque, M.; Al-Ashouri, A.; Korb, P.; Tockhorn, P.; Abate, A.; et al. Co-evaporated formamidinium lead iodide based perovskites with 1000 h constant stability for fully textured monolithic perovskite/silicon tandem solar cells. *Adv. Energy Mater.* **2021**, *11*, 2101460. [CrossRef]
77. Li, Y.; Shi, B.; Xu, Q.; Yan, L.; Ren, N.; Chen, Y.; Han, W.; Huang, Q.; Zhao, Y.; Zhang, X. Wide bandgap interface layer induced stabilized perovskite/silicon tandem solar cells with stability over ten thousand hours. *Adv. Energy Mater.* **2021**, *11*, 2102046. [CrossRef]
78. Isikgor, F.H.; Furlan, F.; Liu, J.; Ugur, E.; Eswaran, M.K.; Subbiah, A.S.; Yengel, E.; De Bastiani, M.; Harrison, G.T.; Zhumagali, S.; et al. Concurrent cationic and anionic perovskite defect passivation enables 27.4% perovskite/silicon tandems with suppression of halide segregation. *Joule* **2021**, *5*, 1566–1586. [CrossRef]
79. Subbiah, A.S.; Isikgor, F.H.; Howells, C.T.; De Bastiani, M.; Liu, J.; Aydin, E.; Furlan, F.; Allen, T.G.; Xu, F.; Zhumagali, S.; et al. High-performance perovskite single-junction and textured perovskite/silicon tandem solar cells via slot-die-coating. *ACS Energy Lett.* **2020**, *5*, 3034–3040. [CrossRef]
80. Chen, B.; Yu, Z.J.; Manzoor, S.; Wang, S.; Weigand, W.; Yu, Z.; Yang, G.; Ni, Z.; Dai, X.; Homan, Z.C.; et al. Blade-coated perovskites on textured silicon for 26%-efficient monolithic perovskite/silicon tandem solar cells. *Joule* **2020**, *4*, 850–864. [CrossRef]
81. Zhumagali, S.; Isikgor, F.H.; Maity, P.; Yin, J.; Ugur, E.; De Bastiani, M.; Subbiah, A.S.; Mirabelli, A.J.; Azmi, R.; Harrison, G.T.; et al. Linked nickel oxide/perovskite interface passivation for high-performance textured monolithic tandem solar cells. *Adv. Energy Mater.* **2021**, *11*, 2101662. [CrossRef]
82. Santbergen, R.; Vogt, M.R.; Mishima, R.; Hino, M.; Uzu, H.; Adachi, D.; Yamamoto, K.; Zeman, M.; Isabella, O. Ray-optics study of gentle non-conformal texture morphologies for perovskite/silicon tandems. *Opt. Express* **2022**, *30*, 5608–5617. [CrossRef]
83. Hou, F.; Han, C.; Isabella, O.; Yan, L.; Shi, B.; Chen, J.; An, S.; Zhou, Z.; Huang, W.; Ren, H.; et al. Inverted pyramidally-textured PDMS antireflective foils for perovskite/silicon tandem solar cells with flat top cell. *Nano Energy* **2019**, *56*, 234–240. [CrossRef]
84. Tockhorn, P.; Sutter, J.; Cruz, A.; Wagner, P.; Jäger, K.; Yoo, D.; Lang, F.; Grischek, M.; Li, B.; Li, J.; et al. Nano-optical designs for high-efficiency monolithic perovskite–silicon tandem solar cells. *Nat. Nanotechnol.* **2022**, *17*, 1214–1221. [CrossRef]
85. Razzaq, A.; Allen, T.G.; Liu, W.; Liu, Z.; De Wolf, S. Silicon heterojunction solar cells: Techno-economic assessment and opportunities. *Joule* **2022**, *6*, 514–542. [CrossRef]
86. Yang, C.; Yu, M.; Chen, D.; Zhou, Y.; Wang, W.; Li, Y.; Lee, T.-C.; Yun, D. An annealing-free aqueous-processed anatase TiO_2 compact layer for efficient planar heterojunction perovskite solar cells. *Chem. Commun.* **2017**, *53*, 10882–10885. [CrossRef]
87. Möllmann, A.; Gedamu, D.; Vivo, P.; Frohnhoven, R.; Stadler, D.; Fischer, T.; Ka, I.; Steinhorst, M.; Nechache, R.; Rosei, F.; et al. Highly Compact TiO_2 Films by Spray Pyrolysis and Application in Perovskite Solar Cells. *Adv. Eng. Mater.* **2019**, *21*, 1801196. [CrossRef]
88. Kavan, L. Electrochemistry and perovskite photovoltaics. *Curr. Opin. Electrochem.* **2018**, *11*, 122–129. [CrossRef]
89. Zhao, Y.; Nardes, A.M.; Zhu, K. Mesoporous perovskite solar cells: Material composition, charge-carrier dynamics, and device characteristics. *Faraday Discuss.* **2014**, *176*, 301–312. [CrossRef]
90. Shahiduzzaman, M.; Saluma, T.; Kaneko, T.; Tomita, K.; Isomura, M.; Taima, T.; Umezu, S.; Iwamori, S. Oblique Electrostatic Inkjet-Deposited TiO_2 Electron Transport Layers for Efficient Planar Perovskite Solar Cells. *Sci. Rep.* **2019**, *9*, 19494. [CrossRef]
91. Su, T.-S.; Hsieh, T.-Y.; Hong, C.-Y.; Wei, T.-C. Electrodeposited Ultrathin TiO_2 Blocking Layers for Efficient Perovskite Solar Cells. *Sci. Rep.* **2015**, *5*, 16098. [CrossRef]
92. Huckaba, A.J.; Lee, Y.; Xia, R.; Paek, S.; Bassetto, V.C.; Oveisi, E.; Lesch, A.; Kinge, S.; Dyson, P.J.; Girault, H.; et al. Inkjet-Printed Mesoporous TiO_2 and Perovskite Layers for High Efficiency Perovskite Solar Cells. *Energy Technol.* **2019**, *7*, 317–324. [CrossRef]
93. Hu, H.; Dong, B.; Hu, H.; Chen, F.; Kong, M.; Zhang, Q.; Luo, T.; Zhao, L.; Guo, Z.; Li, J.; et al. Atomic Layer Deposition of TiO_2 for a High-Efficiency Hole-Blocking Layer in Hole-Conductor-Free Perovskite Solar Cells Processed in Ambient Air. *ACS Appl. Mater. Interfaces* **2016**, *8*, 17999–18007. [CrossRef] [PubMed]
94. Ren, X.; Xie, L.; Kim, W.B.; Lee, D.G.; Jung, H.S.; Liu, S. Chemical Bath Deposition of Co-Doped TiO_2 Electron Transport Layer for Hysteresis-Suppressed High-Efficiency Planar Perovskite Solar Cells. *RRL Solar* **2019**, *3*, 1900176. [CrossRef]
95. Alberti, A.; Smecca, E.; Sanzaro, S.; Bongiorno, C.; Giannazzo, F.; Mannino, G.; La Magna, A.; Liu, M.; Vivo, P.; Listorti, A.; et al. Nanostructured TiO_2 Grown by Low-Temperature Reactive Sputtering for Planar Perovskite Solar Cells. *ACS Appl. Energy Mater.* **2019**, *2*, 6218–6229. [CrossRef]
96. Shahiduzzaman, M.; Kuwahara, D.; Nakano, M.; Karakawa, M.; Takahashi, K.; Nunzi, J.-M.; Taima, T. Low-Temperature Processed TiO_x Electron Transport Layer for Efficient Planar Perovskite Solar Cells. *Nanomaterials* **2020**, *10*, 1676. [CrossRef]
97. Albrecht, S.; Saliba, M.; Correa Baena, J.P.; Lang, F.; Kegelmann, L.; Mews, M.; Steier, L.; Abate, A.; Rappich, J.; Korte, L.; et al. Monolithic perovskite/silicon-heterojunction tandem solar cells processed at low temperature. *Energy Environ. Sci.* **2016**, *9*, 81–88. [CrossRef]
98. Kakavelakis, G.; Maksudov, T.; Konios, D.; Paradisanos, I.; Kioseoglou, G.; Stratakis, E.; Kymakis, E. Efficient and Highly Air Stable Planar Inverted Perovskite Solar Cells with Reduced Graphene Oxide Doped PCBM Electron Transporting Layer. *Adv. Energy Mater.* **2016**, *7*, 1602120. [CrossRef]

99. Werner, J.; Weng, C.H.; Walter, A.; Fesquet, L.; Seif, J.P.; De Wolf, S.; Niesen, B.; Ballif, C. Efficient Monolithic Perovskite/Silicon Tandem Solar Cell with Cell Area >1 cm^2. *J. Phys. Chem. Lett.* **2016**, *7*, 161–166. [CrossRef] [PubMed]
100. Liu, P.; Liu, X.; Lyu, L.; Xie, H.; Zhang, H.; Niu, D.; Huang, H.; Bi, C.; Xiao, Z.; Huang, J.; et al. Interfacial electronic structure at the $CH_3NH_3PbI_3/MoO_x$ interface. *Appl. Phys. Lett.* **2015**, *106*, 193903. [CrossRef]
101. Chapa, M.; Alexandre, M.F.; Mendes, M.J.; Aguas, H.; Fortunato, E.; Martins, R. All thin-film perovskite/C-Si four-terminal tandems: Interlayer and intermediate contacts optimization. *ACS Appl. Energy Mater.* **2019**, *2*, 3979–3985. [CrossRef]
102. Zhao, D.; Ding, L. All-perovskite tandem structures shed light on thin-film photovoltaics. *Sci. Bull.* **2020**, *65*, 1144–1146. [CrossRef]
103. Xu, K.; Al-Ashouri, A.; Peng, Z.; Köhnen, E.; Hempel, H.; Akhundova, F.; Marquez, J.A.; Tockhorn, P.; Shargaieva, O.; Ruske, F.; et al. Slot-Die Coated Triple-Halide Perovskites for Efficient and Scalable Perovskite/Silicon Tandem Solar Cells. *ACS Energy Lett.* **2022**, *7*, 3600–3611. [CrossRef] [PubMed]
104. Zeng, J.; Bi, L.; Cheng, Y.; Xu, B.; Jen, A.K.-Y. Self-assembled monolayer enabling improved buried interfaces in blade-coated perovskite solar cells for high efficiency and stability. *Nano Res. Energy* **2022**, *1*, e9120004. [CrossRef]
105. Chu, L.; Zhai, S.; Ahmad, W.; Zhang, J.; Zang, Y.; Yan, W.; Li, Y. High-performance large-area perovskite photovoltaic modules. *Nano Res. Energy* **2022**, *1*, e9120024. [CrossRef]
106. Kothandaraman, R.K.; Lai, H.; Aribia, A.; Nishiwaki, S.; Siegrist, S.; Krause, M.; Zwirner, Y.; Sevilla, G.T.; Artuk, K.; Wolff, C.M.; et al. Laser Patterned Flexible 4T Perovskite-Cu(In,Ga)Se_2 Tandem Mini-module with Over 18% Efficiency. *RRL Solar* **2022**, *6*, 2200392. [CrossRef]
107. Salah, M.M.; Zekry, A.; Shaker, A.; Abouelatta, M.; Mousa, M.; Saeed, A. Investigation of electron transport material-free perovskite/CIGS tandem solar cell. *Energies* **2022**, *15*, 6326. [CrossRef]
108. Lang, F.; Jost, M.; Bundesmann, J.; Denker, A.; Albrecht, S.; Landi, G.; Neitzert, H.-C.; Rappich, J.; Nickel, N.H. Efficient Minority Carrier Detrapping Mediating the Radiation Hardness of Triple-Cation Perovskite Solar Cells under Proton Irradiation. *Energy Environ. Sci.* **2019**, *12*, 1634–1647. [CrossRef]
109. Brown, C.R.; Eperon, G.E.; Whiteside, V.R.; Sellers, I.R. Potential of High-Stability Perovskite Solar Cells for Low-Intensity–Low-Temperature (LILT) Outer Planetary Space Missions. *ACS Appl. Energy Mater.* **2018**, *2*, 814–821. [CrossRef]
110. Kaltenbrunner, M.; Adam, G.; Głowacki, E.D.; Drack, M.; Schwödiauer, R.; Leonat, L.; Apaydin, D.H.; Groiss, H.; Scharber, M.C.; White, M.S.; et al. Flexible high power-per-weight perovskite solar cells with chromium oxide–metal contacts for improved stability in air. *Nat. Mater.* **2015**, *14*, 1032. [CrossRef] [PubMed]
111. Otte, K.; Makhova, L.; Braun, A.; Konovalov, I. Flexible Cu(In,Ga)Se_2 thin-film solar cells for space application. *Thin Solid Films* **2006**, *511–512*, 613–622. [CrossRef]
112. Todorov, T.; Gershon, T.; Gunawan, O.; Lee, Y.S.; Sturdevant, C.; Chang, L.; Guha, S. Monolithic Perovskite-CIGS Tandem Solar Cells via In Situ Band Gap Engineering. *Adv. Energy Mater.* **2015**, *5*, 1500799. [CrossRef]
113. Guchhait, A.; Dewi, H.A.; Leow, S.W.; Wang, H.; Han, G.; Suhaimi, F.B.; Mhaisalkar, S.; Wong, L.H.; Mathews, N. Over 20% Efficient CIGS–Perovskite Tandem Solar Cells. *ACS Energy Lett.* **2017**, *2*, 807–812. [CrossRef]
114. Boukortt, N.E.I.; Patanè, S.; Garcia Loureiro, A.; AlAmri, A.M.; Abdulraheem, Y.M.; Lenka, T.R.; Paul, R.; Abushattal, A. Electrical and Optical Investigation of 2T–Perovskite/u-CIGS Tandem Solar Cells With ~30% Efficiency. *IEEE Trans. Electron Devices* **2022**, *69*, 3798–3806. [CrossRef]
115. Jošt, M.; Köhnen, E.; Al-Ashouri, A.; Bertram, T.; Tomšič, Š.; Magomedov, A.; Kasparavicius, E.; Kodalle, T.; Lipovsek, B.; Getautis, V.; et al. Perovskite/CIGS Tandem Solar Cells: From Certified 24.2% toward 30% and beyond. *ACS Energy Lett.* **2022**, *7*, 1298–1307. [CrossRef]
116. Kodalle, T.; Bertram, T.; Schlatmann, R.; Kaufmann, C.A. Effectiveness of an RbF Post Deposition Treatment of CIGS Solar Cells in Dependence on the Cu Content of the Absorber Layer. *IEEE J. Photovolt.* **2019**, *9*, 1839–1845. [CrossRef]
117. Saliba, M.; Correa-Baena, J.P.; Wolff, C.M.; Stolterfoht, M.; Phung, N.; Albrecht, S.; Neher, D.; Abate, A. How to Make over 20% Efficient Perovskite Solar Cells in Regular (n−i−p) and Inverted (p−i−n) Architectures. *Chem. Mater.* **2018**, *30*, 4193–4201. [CrossRef]
118. Kim, D.H.; Muzzillo, C.P.; Tong, J.; Palmstrom, A.F.; Larson, B.W.; Choi, C.; Harvey, S.P.; Glynn, S.; Whitaker, J.B.; Zhang, F.; et al. Bimolecular Additives Improve Wide-Band-Gap Perovskites for Efficient Tandem Solar Cells with CIGS. *Joule* **2019**, *3*, 1734–1745. [CrossRef]
119. Nakamura, M.; Lin, C.C.; Nishiyama, C.; Tada, K.; Bessho, T.; Segawa, H. Semi-transparent Perovskite Solar Cells for Four-Terminal Perovskite/CIGS Tandem Solar Cells. *ACS Appl. Energy Mater.* **2022**, *5*, 8103–8111. [CrossRef]
120. Pisoni, S.; Fu, F.; Feurer, T.; Makha, M.; Bissig, B.; Nishiwaki, S.; Tiwari, A.N.; Buecheler, S. Flexible NIR-transparent perovskite solar cells for all-thin-film tandem photovoltaic devices. *J. Mater. Chem. A* **2017**, *5*, 13639–13647. [CrossRef]
121. Pisoni, S.; Carron, R.; Moser, T.; Feurer, T.; Fu, F.; Nishiwaki, S.; Tiwari, A.N.; Buecheler, S. Tailored lead iodide growth for efficient flexible perovskite solar cells and thin-film tandem devices. *NPG Asia Mater.* **2018**, *10*, 1076–1085. [CrossRef]
122. Wu, Z.; Liu, X.; Zhong, H.; Wu, Z.; Chen, H.; Su, J.; Xu, Y.; Wang, X.; Li, X.; Lin, H. Natural Amino Acid Enables Scalable Fabrication of High-Performance Flexible Perovskite Solar Cells and Modules with Areas over 300 cm^2. *Small Methods* **2022**, *6*, 2200669. [CrossRef]
123. Paetzolda, U.W.; Jaysankara, M.; Gehlhaara, R.; Ahlswedec, E.; Paetelc, S.; Qiu, W.; Bastos, J.; Rakocevic, L.; Richards, B.S.; Aernouts, T.; et al. Scalable Perovskite/CIGS Thin-Film Solar Module with Power Conversion Efficiency of 17.8%. *J. Mater. Chem. A* **2017**, *20*, 9897–9906. [CrossRef]

124. Gao, Y.; Liu, C.; Xie, Y.; Guo, R.; Zhong, X.; Ju, H.; Qin, L.; Jia, P.; Wu, S.; Schropp, R.E.I.; et al. Can Nanosecond Laser Achieve High-Performance Perovskite Solar Modules with Aperture Area Efficiency Over 21%? *Adv. Energy Mater.* **2022**, *12*, 2202287. [CrossRef]
125. Zhao, D.; Chen, C.; Wang, C.; Junda, M.M.; Song, Z.; Grice, C.R.; Yu, Y.; Li, C.; Subedi, B.; Podraza, N.J.; et al. Efficient two-terminal all-perovskite tandem solar cells enabled by high-quality low-bandgap absorber layers. *Nat. Energy* **2018**, *3*, 1093–1100. [CrossRef]
126. Forgács, D.; Gil-Escrig, L.; Perez-Del-Rey, D.; Momblona, C.; Werner, J.; Niesen, B.; Ballif, C.; Sessolo, M.; Bolink, H.J. Efficient monolithic perovskite/perovskite tandem solar cells. *Adv. Energy Mater.* **2017**, *7*, 1602121. [CrossRef]
127. Hossain, M.I.; Qarony, W.; Ma, S.; Zeng, L.; Knipp, D.; Tsang, Y.H. Perovskite/silicon tandem solar cells: From detailed balance limit calculations to photon management. *Nano-Micro Lett.* **2019**, *11*, 58. [CrossRef]
128. Bremner, S.P.; Levy, M.Y.; Honsberg, C.B. Analysis of tandem solar cell efficiencies under am1.5G spectrum using a rapid flux calculation method. *Prog. Photovolt. Res. Appl.* **2008**, *16*, 225–233. [CrossRef]
129. Ávila, J.; Momblona, C.; Boix, P.; Sessolo, M.; Anaya, M.; Lozano, G.; Vandewal, K.; Miguez, H.; Bolink, H.J. High voltage vacuum-deposited $CH_3NH_3PbI_3$–$CH_3NH_3PbI_3$ tandem solar cells. *Energy Environ. Sci.* **2018**, *11*, 3292. [CrossRef]
130. Chang, C.-Y.; Tsai, B.-C.; Hsiao, Y.-C.; Lin, M.-Z.; Meng, H.-F. Solution-processed conductive interconnecting layer for highly-efficient and long-term stable monolithic perovskite tandem solar cells. *Nano Energy* **2019**, *55*, 354–367. [CrossRef]
131. Jiang, F.; Liu, T.; Luo, B.; Tong, J.; Qin, F.; Xiong, S.; Li, Z.; Zhou, Y. A two-terminal perovskite/perovskite tandem solar cell. *J. Mater. Chem. A* **2016**, *4*, 1208. [CrossRef]
132. Lin, R.; Xiao, K.; Qin, Z.; Han, Q.; Zhang, C.; Wei, M.; Saidaminov, M.I.; Gao, Y.; Xu, J.; Xiao, M.; et al. Monolithic all-perovskite tandem solar cells with 24.8% efficiency exploiting comproportionation to suppress Sn(ii) oxidation in precursor ink. *Nat. Energy* **2019**, *4*, 864–873. [CrossRef]
133. Palmstrom, A.F.; Eperon, G.E.; Leijtens, T.; Prasanna, R.; Habisreutinger, S.N.; Nemeth, W.; Gaulding, E.A.; Dunfield, S.P.; Reese, M.; Nanayakkara, S.; et al. Enabling Flexible All-Perovskite Tandem Solar. *Joule* **2019**, *3*, 2193. [CrossRef]
134. Leijtens, T.; Prasanna, R.; Bush, K.A.; Eperon, G.E.; Raiford, J.A.; Gold-Parker, A.; Wolf, E.J.; Swifter, S.A.; Boyd, C.C.; Wang, H.P.; et al. Tin–lead halide perovskites with improved thermal and air stability for efficient all-perovskite tandem solar cells. *Sustain. Energy Fuels* **2018**, *2*, 2450. [CrossRef]
135. Eperon, G.E.; Leijtens, T.; Bush, K.A.; Prasanna, R.; Green, T.; Wang, J.T.W.; McMeekin, D.P.; Volonakis, G.; Milot, R.L.; May, R.; et al. Perovskite-perovskite tandem photovoltaics with optimized band gaps. *Science* **2016**, *354*, 861–865. [CrossRef] [PubMed]
136. Rajagopal, A.; Yang, Z.; Jo, S.B.; Braly, I.L.; Liang, P.-W.; Hillhouse, H.W.; Jen, A.K.-Y. Highly Efficient Perovskite–Perovskite Tandem Solar Cells Reaching 80% of the Theoretical Limit in Photovoltage. *Adv. Mater.* **2017**, *29*, 1702140. [CrossRef]
137. Heo, J.H.; Im, S.H. $CH_3NH_3PbBr_3$–$CH_3NH_3PbI_3$ Perovskite–Perovskite Tandem Solar Cells with Exceeding 2.2V Open Circuit Voltage. *Adv. Mater.* **2016**, *28*, 5121–5125. [CrossRef]
138. Heo, J.H.; Im, S.H. $CH_3NH_3PbI_3$/poly-3-hexylthiophen perovskite mesoscopic solar cells: Performance enhancement by Li-assisted hole conduction. *Phys. Status Solidi RRL* **2014**, *8*, 816–821. [CrossRef]
139. Hossain, M.I.; Saleque, A.M.; Ahmed, S.; Saidjafarzoda, I.; Shahiduzzaman, M. Perovskite/perovskite planar tandem solar cells: A comprehensive guideline for reaching energy conversion efficiency beyond 30%. *Nano Energy* **2021**, *79*, 105400. [CrossRef]
140. Wang, J.-Y.; Lee, C.-Y.; Chen, Y.-T.; Chen, C.-T.; Chen, Y.-L.; Lin, C.-F.; Chen, Y.-F. Double side electroluminescence from p-NiO/n-ZnO nanowire heterojunctions. *Appl. Phys. Lett.* **2009**, *95*, 131117. [CrossRef]
141. Forin, C.C.; Purica, M.; Budianu, E.; Schiopu, P. p-NiO/ITO transparent heterojunction- Preparation and characterization. In Proceedings of the International Semiconductor Conference IEEE, Sinaia, Romania, 15–17 October 2012; pp. 131–134.
142. Hossain, M.I.; Qarony, W.; Jovanov, V.; Tsang, Y.H.; Knipp, D. Nanophotonic design of perovskite/silicon tandem solar cells. *J. Mater. Chem. A* **2018**, *6*, 3625–3633. [CrossRef]
143. Xie, F.; Dong, G.; Wua, M.; Wua, K.; Huang, C.; Du, S.; Li, Y.; Wei, M.; Chen, C. Iodine-doped g-C_3N_4 modified zinc titanate electron transporting layer for highly efficient perovskite solar cells. *J. Colloid Interface Sci.* **2023**, *635*, 159–166. [CrossRef]
144. Kirchartz, T.; Rau, U. What makes a good solar cell? *Adv. Energy Mater.* **2018**, *8*, 1703385. [CrossRef]
145. Kirchartz, T.; Bisquert, J.; Mora-Sero, I.; Garcia-Belmonte, G. Classification of solar cells according to mechanisms of charge separation and charge collection. *Phys. Chem. Chem. Phys.* **2015**, *17*, 4007–4014. [CrossRef] [PubMed]
146. Ni, Z.; Bao, C.; Liu, Y.; Jiang, Q.; Wu, W.; Chen, S.; Dai, X.; Chen, B.; Hartweg, B.; Yu, Z.; et al. Resolving spatial and energetic distributions of trap states in metal halide perovskite solar cells. *Science* **2021**, *371*, 1352–1358. [CrossRef] [PubMed]
147. Yang, Y.; Yang, M.; Moore, D.T.; Yan, Y.; Miller, E.M.; Zhu, K.; Beard, M.C. Top and bottom surfaces limit carrier lifetime in lead iodide perovskite films. *Nat. Energy* **2017**, *2*, 16207. [CrossRef]
148. Ricciarelli, D.; Meggiolaro, D.; Ambrosio, F.; De Angelis, F. Instability of Tin Iodide Perovskites: Bulk p-Doping versus Surface Tin Oxidation. *ACS Energy Lett.* **2020**, *5*, 2787–2795. [CrossRef]
149. Savill, K.J.; Ulatowski, A.M.; Herz, L.M. Optoelectronic Properties of Tin–Lead Halide Perovskites. *ACS Energy Lett.* **2021**, *6*, 2413–2426. [CrossRef]
150. Li, C.; Song, Z.; Chen, C.; Xiao, C.; Subedi, B.; Harvey, S.P.; Shrestha, N.; Subedi, K.K.; Chen, L.; Liu, D.; et al. Low-bandgap mixed tin–lead iodide perovskites with reduced methylammonium for simultaneous enhancement of solar cell efficiency and stability. *Nat. Energy* **2020**, *5*, 768–776. [CrossRef]
151. Aydin, E.; Bastiani, M.; Wolf, S. Defect and contact passivation for perovskite solar cells. *Adv. Mater.* **2019**, *31*, 1900428. [CrossRef]

152. Gong, C.; Zhang, C.; Zhuang, Q.; Li, H.; Yang, H.; Chen, J.; Zang, Z. Stabilizing Buried Interface via Synergistic Effect of Fluorine and Sulfonyl Functional Groups Toward Efficient and Stable Perovskite Solar Cells. *Nano-Micro Lett.* **2023**, *15*, 17. [CrossRef]
153. Lin, R.; Xu, J.; Wei, M.; Wang, Y.; Qin, Z.; Liu, Z.; Wu, J.; Xiao, K.; Chen, B.; Park, S.M.; et al. All-perovskite tandem solar cells with improved grain surface passivation. *Nature* **2022**, *603*, 73–78. [CrossRef]
154. Tong, J.; Jiang, Q.; Zhang, F.; Kang, S.B.; Kim, D.H.; Zhu, K. Understanding and suppressing non-radiative losses in methylammonium-free wide-bandgap perovskite solar cells. *Energy Environ. Sci.* **2022**, *15*, 714–726.
155. Stolterfoht, M.; Caprioglio, P.; Wolff, C.M.; Márquez, J.A.; Nordmann, J.; Zhang, S.; Rothhardt, D.; Hormann, U.; Amir, Y.; Redinger, A.; et al. The impact of energy alignment and interfacial recombination on the internal and external open-circuit voltage of perovskite solar cells. *Energy Environ. Sci.* **2019**, *12*, 2778–2788. [CrossRef]
156. Stranks, S.D.; Hoye, R.L.Z.; Di, D.; Friend, R.H.; Deschler, F. The physics of light emission in halide perovskite devices. *Adv. Mater.* **2019**, *31*, 1803336. [CrossRef] [PubMed]
157. Warby, J.; Zu, F.; Zeiske, S.; Gutierrez-Partida, E.; Frohloff, L.; Kahmann, S.; Frohna, K.; Mosconi, E.; Radicchi, E.; Lang, F.; et al. Understanding Performance Limiting Interfacial Recombination in pin Perovskite Solar Cells. *Adv. Energy Mater.* **2022**, *12*, 2103567. [CrossRef]
158. Stolterfoht, M.; Wolff, C.M.; Márquez, J.A.; Zhang, S.; Hages, C.J.; Rothhardt, D.; Albrecht, S.; Burn, P.L.; Meredith, P.; Unold, T.; et al. Visualization and suppression of interfacial recombination for high-efficiency large-area pin perovskite solar cells. *Nat. Energy* **2018**, *3*, 847–854. [CrossRef]
159. Zhao, T.; Chueh, C.; Chen, Q.; Rajagopal, A.; Jen, A.K.-Y. Defect passivation of organic-inorganic hybrid perovskites by diammonium iodide toward high-performance photovoltaic devices. *ACS Energy Lett.* **2016**, *4*, 757–763. [CrossRef]
160. Jiang, Q.; Zhao, Y.; Zhang, X.; Yang, X.; Chen, Y.; Chu, Z.; Ye, Q.; Li, X.; Yin, Z.; You, J. Surface passivation of perovskite film for efficient solar cells. *Nat. Photon.* **2019**, *13*, 460–466. [CrossRef]
161. Zhao, X.; Dong, J.; Wu, D.; Lai, J.; Xu, C.Y.; Yao, Y.; Yang, X.; Tang, X.; Song, Q. Effect of Steric Hindrance of Butylammonium Iodide as Interface Modification Materials on the Performance of Perovskite Solar Cells. *Solar RRL* **2022**, *6*, 2200078. [CrossRef]
162. Chen, H.; Maxwell, A.; Li, C.; Teale, S.; Chen, B.; Zhu, T.; Ugur, E.; Harrison, G.; Grater, L.; Wang, J.; et al. Regulating surface potential maximizes voltage in all-perovskite tandems. *Nature* **2022**, *613*, 676–681. [CrossRef] [PubMed]
163. Alam, M.A.; Khan, M.R. Thermodynamic efficiency limits of classical and bifacial multi-junction tandem solar cells: An analytical approach. *Appl. Phys. Lett.* **2016**, *109*, 173504. [CrossRef]
164. Onno, A.; Rodkey, N.; Asgharzadeh, A.; Manzoor, S.; Yu, Z.J.; Toor, F.; Holman, Z.C. Predicted power output of silicon-based bifacial tandem photovoltaic systems. *Joule* **2020**, *4*, 580–596. [CrossRef]
165. Li, H.; Wang, Y.; Gao, H.; Zhang, M.; Lin, R.; Wu, P.; Xiao, K.; Tan, H. Revealing the output power potential of bifacial monolithic all-perovskite tandem solar cells. *eLight* **2022**, *2*, 21. [CrossRef]
166. De Bastiani, M.; Mirabelli, A.J.; Hou, Y.; Gota, F.; Aydin, E.; Allen, T.G.; Troughton, J.; Subbiah, A.S.; Isikgor, F.H.; Liu, J.; et al. Efficient bifacial monolithic perovskite/silicon tandem solar cells via bandgap engineering. *Nat. Energy* **2021**, *6*, 167–175. [CrossRef]
167. Qasim, U.B.; Saeed, M.M.; Imran, H. Optimization of various terminal topologies of bifacial perovskite/$FeSi_2$ tandem solar cell. *Jpn. J. Appl. Phys.* **2021**, *60*, 104003. [CrossRef]